

2

Nanocrystalline Si EL Devices

B. Gelloz* and N. Koshida

Abstract This review presents the recent developments in electroluminescence (EL) from nanocrystalline silicon systems. These systems include nanoporous silicon, Si-rich silicon oxides and nitrides, superlattices, and other low-dimensional silicon structures. In many of them, EL originates from recombination of excitons in silicon nanocrystals. Systems where nanocrystalline silicon is a key element but is not the luminescent material are also presented. Nanocrystalline silicon can be used for injecting electrons of high energy into a phosphor. It is also useful as sensitizer for efficient excitation of ions such as rare earth ions. Merits and drawbacks of various systems are described. Several tables summarize the performance, in terms of efficiency, stability, emission wavelength, EL threshold, and speed, of the most significant contributions for each device configuration. The most promising devices so far appear to be those including a layer of nanocrystalline silicon doped with rare earth ions, though some devices using the luminescence of Si itself are not far behind.

1. INTRODUCTION

Si technology overwhelmingly dominates microelectronics. However, Si is a very poor light emitting material because of its indirect bandgap. Furthermore, since its bandgap is of 1.1 eV at room temperature (RT), Si cannot emit light in the visible in its bulk crystalline form. As a result, other light emitting materials, such as III–V and II–VI semiconductors, or organic compounds have been chosen for applications in optical communications and displays.

Si-based light emitters are very much desired for several reasons, like overcoming the so-called electrical interconnect bottleneck, by enabling all

Tokyo University of Agriculture and Technology, 2-24-16 Naka-machi, Koganei, Tokyo 184-8588,
Japan bgelloz@cc.tuat.ac.jp

integrated Si optical interconnections. The display community, as well as other arena involving lighting, would also benefit from a cheap, efficient, stable, and integrated Si-based visible light emitter.

The solution could arise from nanostructured Si, where carrier localization and bandgap enlargement make efficient and visible light emission from Si a reality. Recently, rather high photoluminescence (PL) external quantum efficiencies (QEs) have been achieved from nanocrystalline Si (nc-Si) layers, either in the form of Si-rich SiO_x (12% [1]) or porous Si (PS) (23% [2, 3]). The highest EL efficiency reported to date is much lower, just over 1% [4, 5].

Other routes, for infrared emission, include the emission from Er incorporated in Si nanostructures, and carrier confinement induced by local band level fluctuations induced by strain or doping variations.

Despite the large amount of work devoted in the past decade to the fabrication of a practical light-emitting device based on Si, critical problems are still to be overcome. These are poor efficiency (due to leakage or poor injection efficiency), poor stability (due to oxidation or defect generation), the difficulty to obtain green and blue electroluminescence (EL) (due to interface levels within the bandgap), and usually too high operating voltages (due to the high series resistance of nc-Si). However, recent significant progresses in PL and EL efficiency [1–5] and stability [2, 3, 6] are very encouraging. The minimum requirement for the EL external power efficiency is 1% for the least demanding applications.

The purpose of this review is to survey the progresses in the field of nc-Si-based EL. The huge amount of work devoted to PS EL has been reviewed in Sect. 2. Then, the light emission based on ballistic electron excitation was discussed in Sect. 3. In this case, the emitter of electron is PS while the light is usually generated by another luminescent material. Section 4 is devoted to devices including nc-Si in an oxide matrix. In Sect. 5, devices based on other host matrix or nanostructures are presented. These include SiN_x matrix, nanopillars, and nanostructures induced by strain and doping variations. Section 6 deals with EL from superlattices. Section 7 describes the EL from rare earth-doped Si nanoclusters. In Sect. 8, the most significant and promising advances are emphasized.

2. EL OF POROUS SILICON

2.1. *Formation and Properties of Porous Si*

Details about the various properties and formation conditions of PS can be found in various reviews [7–10]. Here, only a very brief overview is given. PS is usually formed by anodization of Si in dilute aqueous or ethanoic HF. PS formation and characteristics depend on several parameters, the most important ones being HF concentration, anodization current density, anodization time, substrate doping density and type, and temperature.

PS can be luminescent only for sufficiently high porosities, in excess of 70%. The useful luminescence band of PS consists in the so-called “S-band.” It originates from exciton recombination into Si nanocrystals, with involvement of surface states

in some cases [11]. This luminescence spectrum is broad (typical FWHM ~ 150 nm) due to nc-Si size distribution. The luminescence efficiency can be improved using various anodization posttreatments such as thermal oxidation, anodic oxidation, chemical oxidation, and chemical or photoassisted dissolution in HF. The PL is usually red-orange. Achieving green and blue PL [12, 13] is difficult due to the presence of surface states introduced by contaminants on PS surface.

The PL lifetimes span from a few nanoseconds in the blue region [14] to several tens of microseconds in the red region. These long lifetimes suggest indirect transition as in bulk Si. It has been confirmed by band structure calculation and spectroscopic characterization [7–10]. The rather long PL lifetimes make difficult high-speed luminescence switching.

Luminescent PS is usually highly resistive due to depletion of free charge carriers as a result of quantum confinement. This makes the charge carrier injection into Si nanocrystals rather difficult.

2.2. Porous Si Impregnated by an Electrolyte

The first demonstration of EL from PS was performed with PS impregnated with a liquid electrolyte [15]. Anodically polarized p-type PS of high porosity in contact with an indifferent conducting liquid phase exhibits efficient and bright EL, visible with naked eye in daylight, at potentials below 2 V. The EL has been attributed to radiative recombination of holes from the Si substrate with electrons resulting from the oxidation of Si atoms at the inner surface of PS [16]. This EL is limited in time because Si nanocrystals are irreversibly oxidized during the process. After an increase, the EL intensity eventually decreases and vanishes [15, 17–20].

Much more stable wet EL has been obtained under cathodic polarization, using the persulfate ($\text{S}_2\text{O}_8^{2-}$) ions [21, 22]. Electrons from the substrate are injected into PS and Si nanocrystals under cathodic bias and induce the reduction of the persulfate ions. The reduction of the $\text{S}_2\text{O}_8^{2-}$ ion is a two-step process. In the second step, hole injection into the Si valence band takes place [23]. Because the two types of charge carriers can be injected in Si nanocrystals, the EL can be generated. Since the Si electrode is not consumed during the process, this EL is more stable than that resulting from anodic oxidation.

Another attractive feature of this system is the voltage-induced spectral shift of the EL [24]. The tunability does not occur only by activation of higher and higher emission energies, but also by simultaneous quenching of the lowest emission energies by Auger effect [25]. Injection of one electron into a luminescent nanocrystal can trigger EL. However, if two or more electrons are injected into a nanocrystal, the nonradiative Auger recombination, dominates, resulting in the quenching of the EL. The quenching of the PL has also been observed [26, 27].

Following the idea of one type of charge carrier injection from the substrate and the other type from a species in the electrolyte, the injection of electrons from the electrolyte has been investigated. Methylviologen [28] and formic acid [29] oxidation lead to electron injection into PS, after capture of holes provided by the substrate. However, this type of EL is not stable due to simultaneous Si oxidation taking place under anodic bias.

2.3. Transport and EL Mechanism in Wet and Dry Porous Si

Relatively high external QE is rather easily achievable with wet PS whereas it is extremely difficult with solid-state PS. Furthermore, the wide voltage-induced tuning of the EL emission band is easily done in wet PS using the reduction of persulfate ions, whereas it is rarely seen in solid-state PS EL devices [30], and not as wide.

In the wet configuration, the conductive liquid impregnates completely the PS skeleton and electrically short circuit the highly resistive PS layer. The current can be limited by any of the three mechanisms (1) the supply of carriers by the substrate (regime 1; EL impossible), (2) the supply of ions by diffusion in the electrolyte (regime 2; EL possible only within a thin layer at the PS surface), or (3) the kinetic of the electrochemical reaction (regime 3; EL possible within the entire PS layer) [31, 32].

When charge carriers can penetrate into PS, their transport is a diffusion process since no significant electric field is set across PS (the electrolyte electrically short circuit PS) [33–35]. Therefore a key feature responsible for the high efficiency and low operating voltages is the absence of an important voltage drop in the liquid-impregnated porous skeleton. Another important characteristic of wet EL is the fact that both electrons and holes can be efficiently injected into Si nanocrystals in part or the whole thickness of PS. Electrons are present in PS, and holes are injected from the electrolyte, in a parallel manner since the liquid impregnates completely the porous network.

In solid-state devices, high voltages are necessary to get a significant current through PS because of the very high series resistance of nano-PS. The resistivity of nano-PS is usually greater than $10^5 \Omega \text{ cm}$ at RT. As a result, high electric fields are set across the PS layer. Locally, the electric field can be high enough to separate the electron–hole pairs, thus seriously limiting the EL efficiency [36]. This is a major difference with the wet configuration.

Another great difference is the charge carrier injection mechanism. Indeed, in dry PS, the charge carrier supply in Si nanocrystals occurs in series and not in parallel. Furthermore, the charge carriers flow preferentially through low resistivity (but non radiative) paths. This reduces considerably the efficiency by shunting luminescent nanocrystals and inducing a large leakage.

The electron–hole pair generation mechanism in most of the solid-state PS-based EL devices can be attributed to an impact process via accelerated electrons through the highly resistive PS skeleton [36]. In contrast, in wet PS, both the electrons and the holes are efficiently injected without the need of high electric fields across PS.

2.4. Devices Including As-Formed Porous Si

Most devices in this paragraph are listed in Table 1. Devices discussed in this section are based on Si/PS/top contact junctions, where the top contact is usually either gold or ITO. The best results are usually obtained with ITO, since it offers good transparency and fair conductivity.

The first true demonstration of injection mode solid-state EL based on PS was reported by Koshida et al. [37] in 1992. The efficiency of this type of devices,

Table 1 Some characteristics of most devices, including a single PS layer, discussed in Sect. 2.4

Contact	Structure	Posttreatment	EL threshold (V mA cm ⁻²)	Stability of EL intensity	Emission peak (nm)	Highest efficiency EQE-EPE (%)	Year	Ref.
Au	p(D)		4–50		680	10 ⁻³	1992	[37]
ITO	p(D)		<2–<10	>5 h	580		1992	[38]
Au or ITO	n(L)		–1	Minutes	700		1992	[40]
Au	n ⁺ (L)		–0.1		680	0.05	1997	[36]
Au	Oxide-free PS from p(D)	L + H ₂ exposure for 12 h			430		1999	[14]

D and L mean that anodization has been conducted in the dark and under illumination, respectively. *ECO* Electrochemical oxidation, *EQE* External quantum efficiency, and *EPE* External power efficiency

without any further treatment, is usually low, i.e., <10⁻³% [37–40], except in one case where 0.05% was obtained [36]. Operating voltages for EL visible in daylight are rather high, usually greater than 10 V.

It is worth noting that blue EL has been demonstrated [14] using an as-formed PS layer formed from p-type Si, with a gold top contact. PS was thinned by using photochemical etching in HF. The efficiency of this device was very low and much work is needed to reach the same level of efficiency as for red-orange emitting devices. Blue emission is difficult to get for several reasons (1) the fabrication of layers with a high density of small nanocrystals is difficult, (2) keeping the nanocrystals oxide-free (to avoid the luminescence red-shift due to introduction of surface states by oxygen) is not an easy task, and (3) charge carrier injection into high energy levels is difficult to get with an appreciable efficiency. The important result of this report [14] is the demonstration of the possibility of RGB LEDs based on Si.

2.5. Porosified pn Junctions

Most devices in this paragraph are listed in Table 2. Devices including a PS layer formed from a pn junction may allow injection of holes and electrons from the two different electrodes. However, it is not sure that true pn junctions can exist in PS. Indeed, free carriers are mostly absent from PS, even when the bulk Si initial doping level is high, and should be trapped on some kind of surface states [41]. As for p-type Si, it seems that dopant atoms are still present in PS at concentration similar to bulk Si, but are passivated [41].

The use of p⁺n junctions, which are made porous by anodization, has provided rather good results. In this configuration, boron atoms are incorporated into an n-type substrate either by implantation or by diffusion. After PS is formed, the top contact is deposited onto the p⁺ side. Devices in which a pn junction is porosified has shown better efficiencies than devices including one Si type only and without any postanodization treatment. p⁺n⁻ [42–48], n⁺p⁻ [49], n⁺p⁺ [50], and p⁺n⁺ [51] junctions have been studied.

Table 2 Some characteristics of most devices, based on porosified pn junction, discussed in Sect. 2.5

Contact	Structure	Posttreatment	EL threshold (V mA cm ⁻²)	Stability of EL intensity	Emission peak (nm)	Highest efficiency EQE-EPE (%)	Year	Ref.
Au	n ⁺ p ⁺ p(D)		<600	>6 h	640	0.18	1993	[50]
Au	p ⁺ n(L)		1.7–0.1	80 h	700	10 ⁻²	1993	[45]
ITO	p ⁺ n(L)	1 min (L)	2.3–10 ⁻³	Hours	600	0.18	1995	[46]
Au	p ⁺ n(L)			Seconds	630	0.16–0.16	1995	[42]
Au	p and p ⁺ n(L)	2 min Exposure in 10% HNO ₃	5		650	0.01	1995	[49]
Au	p ⁺ n(L)		3–1	Seconds	670–780	0.2	1996	[43, 44]
Au	p ⁺ n(L)		>10–10 ⁻³		690	0.8–0.07	1997	[48]
ITO	p ⁺ n ⁺ (L)	ECO	5–1.5 × 10 ⁻⁴	Hours	650	1.1–0.08	1998	[51]

D and L mean that anodization has been conducted in the dark and under illumination, respectively. ECO Electrochemical oxidation, EQE Mean external quantum efficiency, and EPE Mean external power efficiency

Linnros and Lalic have used a porosified np⁺ junction [42–44]. The junction was at a depth of 0.25 μm. Anodization was performed until the total PS thickness was in the range of 20–60 μm. PS from the n-type part is composed of a nanoporous layer at the top and a macroporous underlying layer. EL originates from the n-type part. The device shows high series resistance (due to high PS thickness), inducing high operating voltages and perhaps shunting the pn behavior. The device was pulse-operated. Their best device shows an external QE of about 0.2%.

Nishimura et al. [120] have also used a porosified pn junction. They obtained an external QE as high as 0.8% under pulsed operation, but for high voltages and very low EL intensities.

Simons et al. [52] have used a p⁺n porosified junction. They have made calculations supporting the fact that a pn junction exists in the PS layer included in their device [46], even though the boron implanted atoms were not annealed for electrical activation. The EL is believed to take place in the p⁺n junction. Due to the thin PS layer used (400 nm), their fresh device was CW-operated at voltages below 6 V. The best external QE was 0.18% [46, 52, 53] at 4–6 V and an external QE of about 0.1% was reproducibly achieved. The external QE was highly dependant upon the boron dose. Best performance is found for a dose of about 10¹⁶ cm⁻². The temperature is found especially important for good reproducibility.

Chen et al. [50] have fabricated a device by anodizing an n⁺p⁺p substrate. PS was formed from the n⁺ side and extends up to the p region. The top contact was Au. EL could be seen within a forward voltage of 5–10 V and a current density of approximately 600 mA cm⁻². Rectifying properties were very good. The light originated from a PS region a few micrometers below the top contact–PS interface. The authors then conclude that the EL has to be the result of electron–hole recombination at the porous n⁺p⁺ junction.

Gelloz et al. [51] reported a record external QE of 1.1% (external power efficiency (EPE) of 0.08%) using a porosified p⁺n⁺ junction. The PS layer was about 20 μm. This device also suffered from high voltage operation. In this case, the high external QE was attributed mainly to the postanodization anodic oxidation of PS (described in Sect. 2.6).

2.6. Partially Oxidized Porous Si

Most devices in this paragraph are listed in Table 3. Also see oxidized devices in Table 2. Partially oxidizing PS is useful for two reasons. (1) It reduces the sizes of Si network, inducing an enhancement of the PL QE (via enhanced charge carrier localization and/or creation of new luminescent nanocrystals) and it usually leads to a reduction of the leakage current. (2) The surface of as-formed PS is terminated by Si-H_x (x = 1, 2, 3) bonds, which get oxidized very easily during storage and device operation, inducing a very poor stability. When PS is covered by a thin oxide layer, the stability is generally enhanced. PS oxidation has been conducted under various conditions: chemically [54], thermally [55–57], and electrochemically [4, 51, 58–60].

Kozlowski et al. [54] have oxidized n-type PS in H₂O₂/water/ethanol mixture. This way, EL can be stabilized at about 50% of the initial value for several hours. EQE is found to increase during operation.

One group has oxidized PS using thermal oxidation in the range of 800–900°C, either in N₂ (nominally) or in N₂ with 10% O₂ [55–57]. The device consisted in a porosified p⁺p[−]-type junction. The top contact was a 300-nm thick n⁺ type poly-Si deposited onto the p⁺ side. The resulting device has several advantages. First, the

Table 3 Some characteristics of most devices, based on partially oxidized PS, discussed in Sect. 2.6

Contact	Structure	Posttreatment	EL threshold (V mA cm ^{−2})	Stability of EL inten- sity	Emission peak (nm)	Highest efficiency EQE–EPE (%)	Year	Ref.
Au	n(L)	H ₂ O ₂ oxidation			650–750			[54]
Au	n(UV)	H ₂ O ₂ oxidation		>7 h	460–550			[54]
Al-poly Si	p ⁺ p(D)	Anneal in N ₂	1.5–2	1 Month	620–770	0.1	1996	[55–57]
		Or in 10% O ₂ in N ₂					1997	
ITO	n ⁺ (L)	ECO	3.5–4 × 10 ^{−4}		640	0.51–0.05	1998	[51]
ITO	n ⁺ (L)	ECO	3–10 ^{−4}	Hours	640	0.21–0.02	1998	[58]
ITO	n ⁺ (D)	ECO	2–1.8 × 10 ^{−3}	Hours	680	0.5–0.2	1999	[60]
Al/n ⁺	p(L)	ECO		>1 Week			1999	[59]
ITO	n ⁺ (D)	ECO	2.2–7 × 10 ^{−4}	Days, EQE is stable	680	1.07–0.37	2000	[4]
ITO	n ⁺ (L)							
ITO	n ⁺ p	HWA	2–10 ^{−4}	stable	700	10 ^{−3}	2006	[63]

D and L mean that anodization has been conducted in the dark and under illumination, respectively. ECO Electrochemical oxidation, EQE Mean external quantum efficiency, and EPE Mean external power efficiency

stability is rather good, with weeks of stable EL [57]. Second, the EQE of 0.1% is relatively high [55–57]. Third, the EL can be modulated by a square wave current pulse with frequencies greater than 1 MHz [56]. Finally, a bipolar device fully compatible with conventional Si microelectronic processing has been demonstrated [56, 61]. The high stability is due to the replacement of the fragile hydrogen covering the initial PS surface by a thin Si oxide layer. The increase in response speed may be related to a different recombination mechanism involving the oxide rather than the interior of the Si nanocrystals.

Blue and green EL has been reported from partially oxidized PS. Mimura et al. [62] obtained blue EL from porous SiC layers and green EL from PS formed under UV illumination. In this latter case, the PL and EL spectra were different, and though to have different mechanisms. The efficiency was very low ($<10^{-5}\%$).

Postanodization partial ECO of PS has been studied in a view to increase the efficiency and stability [58]. PS includes nonluminescent weakly confined Si regions through which a large leakage current flows. This is one of the reasons for the low QE of PS-based EL. The objective of ECO is to decrease selectively the size of the non-confined Si skeleton without affecting much the confined Si nanocrystals, in order to reduce the leakage without damaging the luminescence. In addition, ECO performed in appropriate conditions optimizes charge carrier injection into luminescent crystallites.

Figure 1 illustrates the ECO process. Oxidation occurs at the internal surface, where holes supplied by the substrate are injected. During the first stages of the process, hole injection and oxidation, occurs only in nonconfined silicon regions. Hole injection in more energetic levels is later achieved, and injection eventually occurs in low-dimensional luminescent crystallites. EL can be observed at this stage, during the ECO treatment itself. EL reaches a maximum when carrier injection in confined crystallites is optimal.

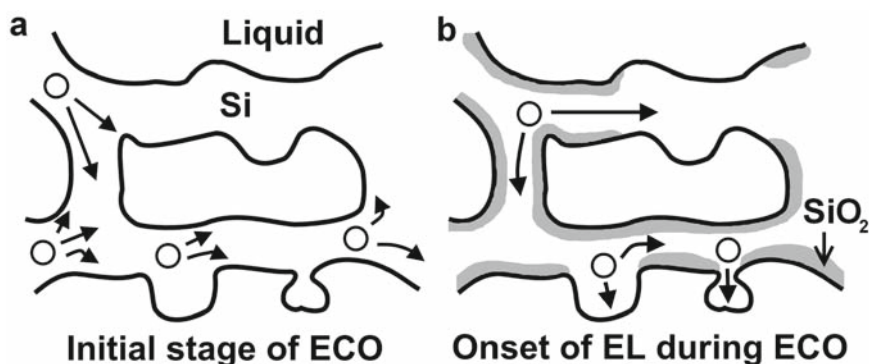


FIG. 1. Schematic representation of the anodic oxidation process in porous silicon under galvanostatic condition. First, holes supplied by the substrate flow through nonconfined silicon (a). Later on, as a result of the oxidation of the surface of nonconfined silicon regions, the potential is increased in order to keep the current constant, and carrier injection into luminescent crystallites becomes possible, inducing the electroluminescence (b).

When oxidation is performed up to the maximum of EL, the nonemissive coarser regions of PS have been significantly oxidized and therefore their sizes have been much reduced, whereas low-dimensional luminescent nanocrystals have only been slightly oxidized and have been well-preserved. ECO decreases the leakage by several orders of magnitude. Thermal or chemical oxidation could not lead to such an enhancement since it occurs almost uniformly on the whole internal surface of PS (without selecting nonconfined silicon from confined silicon). Moreover, contrary to thermal oxidation, ECO does not affect much both the PS structure and the surface passivation with hydrogen [18].

ECO also enhances the luminescence homogeneity. If PS is not uniform, ECO acts as a kind of healing treatment in so far as it tends to homogenize the size distribution of the conductive paths. The EL during ECO is also a unique probe of PS homogeneity.

The strong effect of ECO on the EL efficiency was first demonstrated by Gelloz et al. [58], who obtained an EQE of 0.21% (EPE of 0.02%) with a single PS layer made from n^+ (100) Si. The EL spectrum fits very well the PL one, indicating that the same carrier-recombination mechanism is involved in the two phenomena (recombination of excitons localized within silicon nanocrystallites). EQE of 0.51% and 1.1% (EPE of 0.08%) was then obtained with n^+ (111) and p^+n^+ (111) (p^+ at the surface) PS layers, respectively [51]. However, the operating voltages of these devices were still high, exceeding 10 V. An optimized device, operating below 5 V, with an EQE of 1.07% and an EPE of 0.37% has later been fabricated [4]. The modulation speed was about 33 kHz. Strictly controlled conditions are important for good reproducibility. In particular, the temperature is maintained at 0°C during PS formation of the active PS layer.

Figure 2 shows the EL intensity and the current density as a function of voltage, for two devices [4]. They have been prepared in the same conditions, except that one has been ECO-treated and the other one is not oxidized. EL of oxidized device can be seen with unaided eye in room lighting at operating voltages below 5 V. Since the ECO induces a decrease of the current density of about 3 orders of magnitude and a 10-fold enhancement of EL intensity, the QE of the device is increased by more than 4 orders of magnitude. The dramatic enhancement of EQE of PS EL due to ECO has been confirmed by Pavese et al. [59].

The ECO treatment also improves the EL stability [4, 51, 58]. The device of Gelloz et al. [4] shows no loss of efficiency during operation, and after one-month storage in air. However, the PS layer still gets slowly oxidized during operation and storage in air. Pavese et al. [59] have also applied the ECO on their device and confirmed the enhancement of the stability. No degradation of EL intensity during several days has been obtained. In this case, the conditions used for the ECO have probably led to the growth of an oxide layer which has replaced the initial hydrogen passivation. The ECO treatment had such an impact that it is now used in almost all new EL devices and also in a number of devices based on PS, such as ballistic electron emitters.

Very recently, a new treatment of PS, based on high-pressure water vapor annealing (HWA), has been proposed to enhance the QE and the stability of PS PL

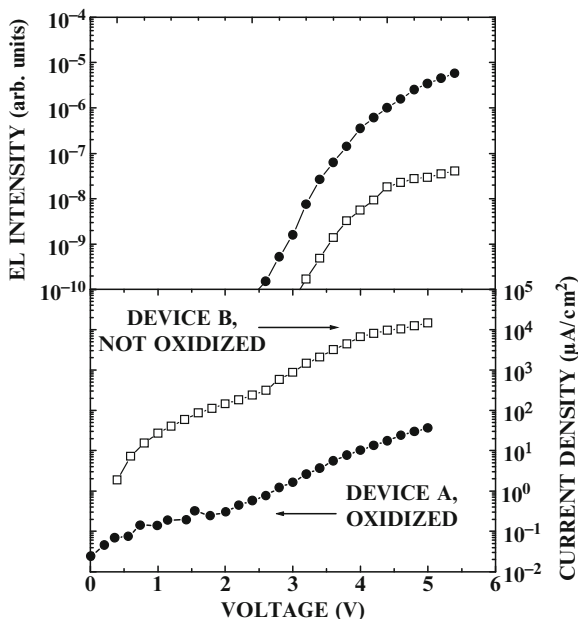


FIG. 2. Electroluminescence intensity and current density as a function of applied voltage for an anodically oxidized (device A) and a not-oxidized device (device B). Reprinted with permission from [4] © 2000 American Institute of Physics [S0021-8979(00)01020-3].

[2, 3]. A record high PL external QE of 23% has been reported, with an outstanding stability under continuous laser excitation, using a pressure of 2.6 MPa at 260°C. The extremely high QE is a result of high exciton localization in nc-Si and extremely reduced nonradiative defect density at the nc-Si/SiO₂ interfaces, the stress in the oxide being very much relaxed compared to that of conventional PS. The application of this technique in EL is currently under investigation and has already shown promising results. In particular, very good stability has been achieved [63].

2.7. Porous Si Impregnated by Another Material

Most devices in this paragraph are listed in Table 4. In order to imitate the efficient wet EL, impregnation of PS with a conductive material, either a metal or a polymer, has been considered.

One group has studied the incorporation of In [47, 64, 65], Al [47], Sn [47, 65], and Sb [47, 65] into PS pores by electrochemical techniques. The best device was obtained with In, with an EQE of 0.01% in ac conditions [47]. The In plating increases the external QE by a factor of 150. PS is also partially oxidized. The mechanism by which the external QE is increased by In electroplating was not fully understood as the oxide was probably also involved. This device emits in the blue (480 nm). This EL may as well be oxide-related rather than the result of exciton recombination in Si nanocrystals.

Table 4 Some characteristics of most devices, based on PS impregnated by another material, discussed in Sect. 2.7.

Contact	Structure	Posttreatment	EL threshold (V mA cm ⁻²)	Stability of EL intensity	Emission peak (nm)	Highest efficiency EQE-EPE (%)	Year	Ref.
Au	p(D)	Polypyrrole electro- deposition	2–<0.01		590		1993, 1995	[66, 67]
Au	n ⁺ (D)	PANI chemical deposition	3–400		800		1995	[68]
Au	n(L)	Polyaniline chemical deposition	–500		790		1996	[69]
Au	n(L:UV)	In electroplat- ing	–0.1	Hours	455–480	0.01	1994– 1997	[47, 64, 65]
Au	n(L:UV)	Ga electro- plating		Hours	520		1996	[65]
Au	n(L:UV)	Sn electroplat- ing		Hours	550	0.0005	1996, 1997	[47, 65]
Au	n(L:UV)	Sb electroplat- ing		Hours	700–750	0.0001	1996, 1997	[47, 65]
Au	n(L:UV)	Al electroplat- ing	–0.1	Hours	480	0.005	1997	[47]

D and L mean that anodization has been conducted in the dark and under illumination, respectively.
EQE Mean external quantum efficiency and EPE Mean external power efficiency

As for polymers, polypyrrole [66, 67] and polyaniline [68, 69] have been used. Efficiency is usually enhanced by the polymer impregnation, but the attempt to imitate completely the liquid contact could not be achieved in any case, the efficiency remaining low. Koshida et al. [66, 67] have studied a device in which polypyrrole had been electrochemically deposited into p-type PS pores and a gold contact deposited onto PS. The current–voltage characteristics and the voltage and current dependence of EL were significantly improved in comparison with a control device. The voltage thresholds of EL are identical whether polymer is incorporated or not. However, the EL intensity as a function of voltage rises in a much steeper way when polymer is used. The EPE is improved by a factor of 3.

Halliday et al. [69] have chemically deposited polyaniline into and onto PS made from n-type Si. The polymer acts as a hole injector. EL is obtained at 0.5 A cm⁻². Bsiey et al. [68] have deposited polyaniline (PANI) into n⁺ PS by chemical oxidation of aniline by persulfate ions. Optimal results are obtained with deposition of two layers of PANI. More layers of PANI reduce the EL intensity. The test device, without polymer shows a voltage threshold of EL of about 9 V. When two PANI layers are deposited in PS, the voltage threshold of EL becomes 3 V and EL intensity increases with a much higher slope than when no polymer is present in PS. However, when more PANI layers are incorporated, the performance of the diode drops, even though it is still better than when no polymer exists in PS. EL

intensity is found six times lower than that from the liquid junction cell. The current–voltage characteristics and the voltage and current dependence of EL were significantly improved in comparison with a control sample including a gold top contact. Li et al. [70] have also deposited polyaniline and found that the EL intensity is increased compared to a control device.

It is worth noting that good impregnation of a material much more conductive than PS could short-circuit the PS layer, resulting in low carrier injection into Si nanocrystals. Such a situation would be similar to regime 1 described in Sect. 2.3 for liquid contact [31, 32], in the sense that the contact would prevent carrier injection from the Si substrate into PS. Solid-state emulation of regime 2 or even better regime 3 of the liquid contacted systems would be a promising approach for enhancing the efficiency.

Filling of the pores with materials that are inert from the electrical and the optical point of view has been proposed to enhance the mechanical stability of the PS skeleton [55]. Various polymers have been tried, such as PVC, polyamide, PMMA, polystyrene, and polypropylene. The hardness of the resulting nanocomposite increased with the density of the base polymer. Maximum increase in hardness achieved is 50%.

2.8. Influence of the Top Contact Configuration

Several devices in this paragraph are listed in Table 5. Oxidized devices can be found in Table 3. Several top contact configurations have been investigated. An ideal contact should be transparent to visible light in order to guarantee maximum light extraction.

Most devices include a thin semitransparent gold or ITO top contact. Simons et al. [71] have compared ITO and gold as top contact. Devices with a semitransparent Au contact were much less stable in air than those with an ITO contact because of the gold layer being more permeable to air than the ITO layer. The devices contacted by gold got oxidized and degraded much faster than those contacted by ITO. The device with ITO exhibited a QE ten times higher than with gold.

Some devices include Al top contacts. In the case of Lazarouk et al. [72, 73], aluminum contact was deposited onto PS. Then, parts of the Al layer were electrochemically oxidized into Al_2O_3 to create transparent windows through which EL was observed. The stability is reported to be more than a month. However, the efficiency is limited by the fact that a significant part of the light cannot be extracted. Moreover, the color emitted by the device was white, leading to the conclusion that the EL probably originated from some oxide-related centers rather than from the nanocrystals cores.

If the top contact is directly deposited onto the rough and uneven surface of a highly porous PS layer, conduction peculiarities may arise and reproducibility can be bad [60]. To solve these problems, some authors [4, 51, 55–57, 60] have included a superficial compact porous layer between the optically active porous layer and the top contact. This superficial layer provides a better electrical contact and greater mechanical stability to the device. In the case of Gelloz et al. [4, 60], the superficial layer consists in a PS layer whose surface conserves the mirror property of the silicon

Table 5 Some characteristics of several devices discussed in Sect. 2.8, about porous Si-based LEDs in which a particular top contact has been used

Contact	Structure	Posttreatment	EL threshold (V mA cm ⁻²)	Stability of EL intensity	Emission peak (nm)	Highest efficiency EQE-EPE (%)	Year	Ref.
ITO/ n-type SiC	p(D)	KOH dip					1992	[78]
Al/Al ₂ O ₃	n or n ⁺ poly		5–400	>1 Month		–0.01	1996	[72, 73]
Au	n poly Si (L)				860–930	0.04	1996	[74]
Au	p ⁺ n(L)			Minutes	700	0.02	1997	[71]
ITO	p ⁺ n(L)			Hours	700	0.2	1997	[71]
Au–Al–pin (a-Si:H)	np(D)				Three peaks: 455, 590, 670	0.13	1997	[75]
Au–Al–npin (a-Si:H)	p(D)		6				1997	[77]
Au–Al–npnin (a-Si:H)	p(D)		3.6				1997	[77]
ITO/a-C	n ⁺ (D) n ⁺ (L)	ECO	0.5	Minutes	Voltage tunable	–0.35	2003	[30]

D and L mean that anodization has been conducted in the dark and under illumination, respectively. ECO Electrochemical oxidation, EQE Mean external quantum efficiency, and EPE Mean external power efficiency

substrate and which is more compact than the underlying active porous layer. In some other cases, a p⁺ PS superficial layer [51, 55–57] is used. PS formed from p⁺ Si shows much better mechanical stability than PS made from other Si substrates. Therefore such layer is a good choice as a buffer layer between the top contact and the active PS layer.

EL colors from red to blue has been obtained by variation of the contact metal [47, 64, 65, 74]. In/Au, Al/Au, Ga/Au, Sn/Au, and Sb/Au contacts lead to EL emission at 455, 455, 520, 555, and 700 nm, respectively [47]. The metals were also impregnated into PS. However, the oxide in the PS layers is believed to be responsible for the short wavelength EL emission.

A 300-nm thick n⁺ poly-Si layer has been used between the Al top contact and PS [55]. This device has already been discussed in Sect. 2.6. The incorporation of the poly-Si layer reduces the surface states concentration at the interface between the PS and the top contact [55].

More sophisticated structures have been considered in a view to enhance the carrier injection into PS. One group has studied devices in which a p–i–n [75] or a n–p–i–n [76] or a n–i–p–n [77] or a n–i–n–p–n [77] a-Si:H multilayer structure has been deposited onto PS. The n–i–n–p–n device has a lower threshold voltage for

EL detection (3.6 V) than the n-i-p-n LED (6 V) [77], which in turn is better than PS LED (>10 V). The a-Si:H multilayer structure is believed to enhance the carrier injection into PS. Red-orange EL can be seen by naked eye in the dark [77]. Brightness of about 30–50 cd m⁻² at 600 mA cm⁻² and an EL efficiency of 0.13% have been reported [75]. The p-i-n PS LED [75] is said to be voltage tunable between 30 and 90 V, as a result of three peaks present in the EL spectrum.

Futagi et al. [78] fabricated a device with microcrystalline SiC deposited onto PS. The diode structure was p-type Si/PS/n-type SiC/ITO. The EL efficiency was very low. The EL was observed by naked eye in the current range from 200 to 619 mA (contact area equals 1 mm²), at a voltage above 20 V.

More recently, Gelloz et al. [30] studied the effect of a few nanometer thick amorphous carbon layer deposited (by sputtering) onto PS before the deposition of the ITO top contact. Visible EL in room lighting was obtained at an operating voltage as low as 3 V from n⁺-Si/ECO-treated thin PS(600 nm thick)/a-C/ITO junctions. A brightness of 3 Cd m⁻² was achieved at 3 V. The EL voltage threshold was below 1 V and about -0.5 V under forward and reverse operation, respectively. The carbon film enhances the stability and the EL efficiency. In addition, the reproducibility from device to device is very much improved by the carbon film. The enhancement in stability is attributed to the capping of PS by the carbon film and the high chemical stability of carbon and Si-C bonds, which should prevent PS oxidation. The carbon film acts as an efficient mechanical and electrical buffer layer between PS and ITO, resulting in enhanced mechanical, electrical, and chemical stability of the top contact. Figure 3 shows that the EL peak wavelength is continuously voltage tunable between 700 and 630 nm for a voltage ranging from 2 to 5 V, a property that is not directly related to the carbon film. This behavior is unique in PS-based EL. It has its origin in the field-induced EL generation mechanism combined with high efficiency [30].

2.9. Stabilization of Porous Si EL by Layer Capping or Surface Modification

Layer capping and encapsulation techniques have been proposed in order to prevent the contamination of PS by all sorts of molecules present in ambient atmosphere. Especially, PS should be protected from water to avoid the ineluctable oxidation that occurs when it is left in air.

The top contact itself could act as a partial capping layer. For example, Simons et al. [71] have shown that semitransparent gold layers are much more permeable to air than thicker ITO layers. More complete capping of PS has been achieved by Lazarouk et al. [72] by using an aluminum layer whose parts were electrochemically oxidized into Al₂O₃ to create transparent windows. The EL was stable for more than a month.

Koshida et al. [79] have studied the capping of ECO-treated PS by electron cyclotron resonance sputtered SiO₂ films. The device was that developed by Gelloz et al. [4] (see Sect. 2.6). The stabilization of the external QE becomes better when the capping layer thickness increases. Two deposition modes were studied: the oxide modes and the metal modes. The metal mode leads to much better stabilization than the oxide mode, because it presents lower permeability to water molecules.

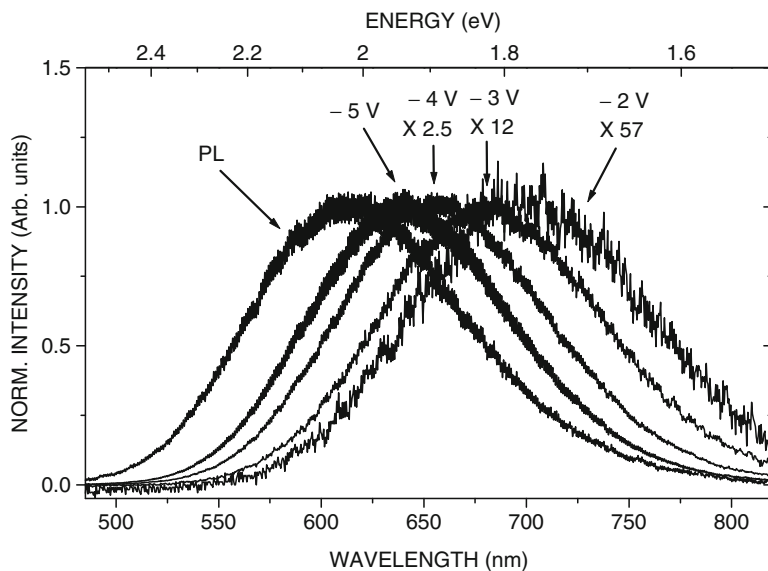


FIG. 3. Normalized PL spectrum and EL spectra at different reverse voltages for a device including a thin porous Si layer and a few nanometer-thick carbon buffer layer between the porous Si layer and the top contact. Reprinted with permission from [30] © 2004 The Japan Society of Applied Physics [DOI: 10.1143/JJAP.43.1981].

The microscopic defects in SiO_2 films deposited by metal mode possibly act as antidiffusion trapping sites for water molecules.

The replacement of the Si–H bonds terminating the PS surface by more stable bonds has been proposed in order to increase the EL stability. EL from deuterium-terminated PS exhibits better stability than hydrogen-terminated PS, but do not solve the problem for the long run [80].

A simple and rather successful approach to stabilize the PS PL has been the replacement of most Si–H bonds at the surface of PS by stable Si–C bonds using hydrosilylation reactions either catalyzed by Lewis acids or thermally activated [81]. The latter process has been successfully implemented for the enhancement of the EL stability [6, 82]. The surface modification was performed by thermal reaction of the PS surface with 1-decene, ethyl-undecylenate, *n*-caprinaldehyde, and undecylenic acid at about 100°C. Figure 4 shows the EL intensity and the current density as a function of time for a not modified reference device and devices including PS layers modified using different molecules, under constant voltage. Modified devices exhibit very good stability whereas the reference device degrades rather quickly. The external QE was somewhat lowered by the modification using 1-decene, ethyl-undecylenate, and *n*-caprinaldehyde, but was well preserved when using undecylenic acid [82]. The enhanced stability was attributed to a better stability of the newly created Si–C or Si–O bonds and by the fact that the long organic groups represented a hydrophobic physical barrier that prevented water molecules and other contaminants from accessing the PS surface, thus preventing PS oxidation.

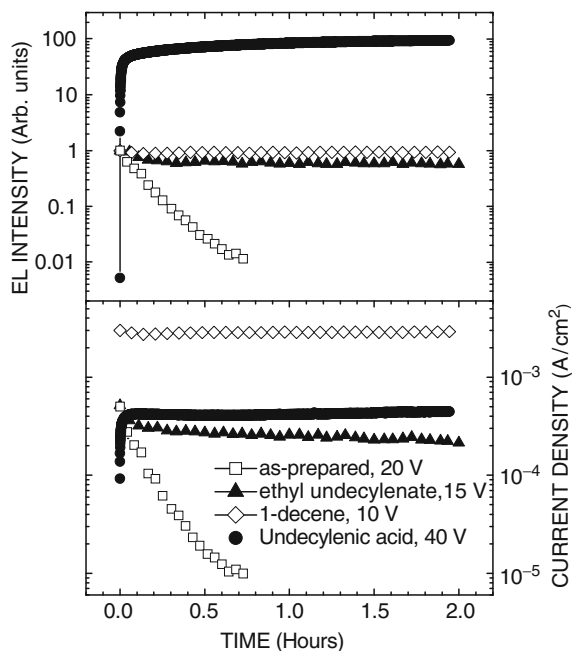


FIG. 4. Current density and normalized EL intensity as a function of time for a reference device and devices treated with various organic molecules. Adapted from [82].

As already discussed in Sect. 2.6, the technique of HWA is a new technique that provides very stable PL [2, 3] and EL [63]. It is a very promising low temperature process.

2.10. Microcavities

Making a microcavity by inserting a luminescent PS layer between two reflective media offers three main advantages. First, a significant PL line narrowing is achievable in this way [83]. Second, high luminescence directionality can be achieved [83, 84]. Finally, although not experimentally demonstrated yet, a reduction of the EL response time is potentially possible by using PS in a microcavity [83] since the PL lifetime may be reduced in this way.

Tuning of the EL emission has been achieved by placing the luminescent PS layer between two multilayer Bragg reflectors (a Fabry-Perot resonator). These Bragg reflectors consist of PS layers of alternating refractive index [83]. Araki et al. [85] used the silver top contact in place of the top reflector and achieved a reduction of the FWHM by a factor of 3. The FWHM was about 100 meV for the emission energy of 1.8 eV. The same group has demonstrated the possible tuning of the PL emission from 1.5 to 2.2 eV [164]. Narrow spectra (10–40 meV in FWHM) are possible by using this approach, compared to the wide typical FWHM of PS PL (≈ 0.25 eV).

Chan et al. [84] demonstrated narrow and tunable EL, depending on the anodization parameters, using an active layer sandwiched between two Bragg

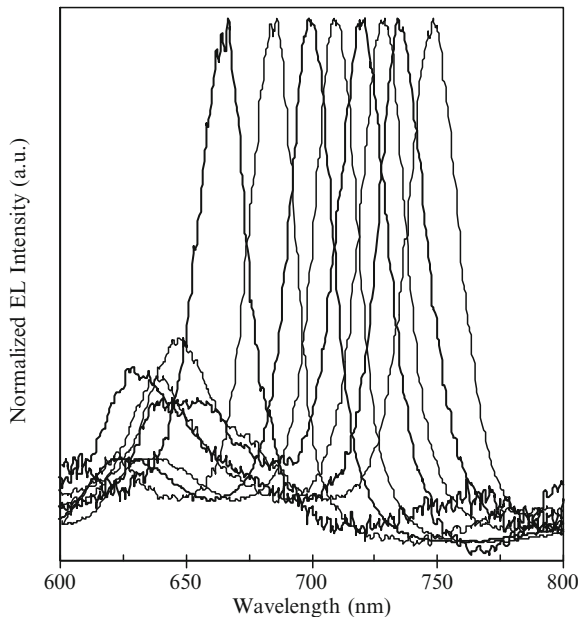


FIG. 5. Electroluminescence from oxidized porous Si microcavity resonators with varying active layer porosity. Devices were reverse biased at about 100 V. Reprinted with permission from [84] © 1999 American Institute of Physics [S0003-6951(99)01828-8].

reflectors. The substrate was p^+ Si. With six periods per mirror, the devices are typically operated at a reverse bias as high as 100 V due to the thick total PS layer involved. The FWHMs were about 50 meV. The EL can be tuned from 1.65 to 1.85 eV (see Fig. 5) by changing the porosity of the active layer from 76 to 94%. In addition, a high directionality of the EL emission was observed in these devices, the emission being concentrated within a 30° cone around the axis. Since PS made from p^+ Si is usually not highly luminescent, these devices were not efficient. The problem is that good quality microcavities are difficult to get with low-doped PS and n-type PS.

2.11. EL Modulation Speed

The decay and rise times of all devices are below the millisecond and do not represent any problem for display applications. However, the modulation speed of all devices is below the GHz, making application in optical interconnects very challenging. The modulation speed is usually influenced by the carrier mobility in PS, the radiative recombination processes, and the charge trapping. The PL decay following pulsed excitation is usually in the microsecond range [7–10].

The EL modulation speed is typically found to be of the order of about ten of microseconds [4, 42–44, 49, 53, 74]. However, one group has reported an efficient (0.1% of external QE) device based on partially oxidized PS that can be modulated at a frequency greater than 1 MHz [56]. The high response speed may

be due to a recombination mechanism that does not involve the interior of the Si nanocrystals. Modulation frequency of 200 MHz has been reported [86] for a device showing lower efficiency and whose EL probably does not originate from recombination of excitons in Si nanocrystals. The device speed was limited by the junction capacitance.

A reduction of the EL response time is potentially possible by using PS in a microcavity [83] since the PL lifetime may be reduced in this way. Another promising route for faster devices is the use of blue luminescence. Indeed, the PL lifetime decreases down to the nanosecond regime for blue emission [14].

2.12. Integration

Besides EL devices, useful optical devices such as optical waveguides [87], optical waveguides on silicon substrates by simple processing. Besides, optical nonlinearity in PS has been demonstrated in a Fabry-Pérot resonator, leading to the availability of PS for optical switches and optical logic gates [92]. Most of these phenomena have only been observed separately (on different substrates). However, progresses have been made in the integration of some of these functions, especially the EL.

A bipolar device fully compatible with conventional Si microelectronic processing has been demonstrated [61]. The EL device was based on thermally oxidized PS. The driving transistor, connected in the common-emitter configuration, could modulate the light emission by amplifying a small base input signal and controlling the current flow through the EL device. The device could be turned on and off by applying a small current pulse to the base of the bipolar transistor. Arrays of such integrated structures have also been fabricated.

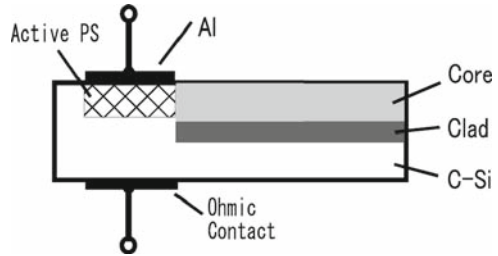
EL from polycrystalline Si and its possible integration in large-area applications have also been demonstrated [93]. Porous polycrystalline Si diodes were shown to operate with efficiencies comparable to that of conventional PS devices. The EL mechanism is believed to be the same in both cases. It has also been confirmed that porous polycrystalline EL devices can be driven by a poly-Si-based switching TFT [93].

The compatibility of PS with silicon-on-insulator technology has been demonstrated [94]. The formation of PS using silicon-on-insulator substrates has been done using an alternating current electrochemical process. The characteristics of the resulting PS layers were similar to that of conventional PS.

Barillo et al. [95] fabricated a PS EL device using a process compatible with an industrial bipolar + complementary MOS + diffusion MOS technology. The device was based on a p/n⁺ junction.

The monolithic integration of a PS EL emitter and a PS-based waveguide, using a simple anodization and standard silicon processing techniques, has been demonstrated [96]. The monolithic integration of an n⁺-type PS-based light emitter and a p-type PS-based waveguide has been achieved using several implantation steps, starting from an n-type Si substrate and a one-step anodization. Figure 6 shows the cross-sectional view of the chip. The EL signal can be transmitted through the optical waveguide and emitted from the edge.

FIG. 6. Schematic representation of a porous Si-based LED integrated with an optical waveguide. The core, clad and LED (active PS field) are formed in a single-step anodization process.



3. EL BASED ON BALLISTIC ELECTRON EXCITATION

3.1. *Electron Emission from Porous Si and Its Mechanism*

Cold electron emission is another useful function of PS diodes [97–105]. The first experimental PS diode consisted of a thin Au film, PS, n^+ -type Si substrate, and ohmic back contact. When a positive voltage is applied to the Au electrode, with respect to the substrate, electrons as well as photons are uniformly emitted through the Au contact.

The PS diode as surface-emitting cold cathode has several advantages compared to conventional cold emitters [106–109]. First, electrons are emitted perpendicularly from the diode surface. Second, the cathode operates at relatively low voltage and third, the emission current is not sensible to ambient pressure.

The emission mechanism has been explained as follows. PS is composed of electrically isolated or interconnected Si nanocrystals surrounded by a thin wide bandgap layer. This latter layer consists in Si oxide. Figure 7 illustrates the electron emission process. Under positive bias, a large potential drop is produced in the PS layer, especially near the PS surface. Electrons are thermally injected from the heavily doped n -type substrate and drifted through PS toward the top contact. In PS, electrons are accelerated especially across regions between Si nanocrystals by multitunneling processes and eventually become ballistic electrons. This process is supported by Fowler–Nordheim analysis, numerical analysis (Monte Carlo) of electron drift length from time-of-flight measurements, and voltage dependence of the energy of emitted electrons [110, 111]. Impact ionization processes occur as well. At sufficiently high bias, the situation near the Au/PS interface can be considered as a state of voltage-controlled negative electron affinity. Electrons in PS near the outer surface by the field-induced carrier generation cascade can be emitted into vacuum through a thin oxide layer and a thin Au film.

3.2. *Optimization of the Electron Emission from Porous Si*

The effect of PS thickness has been studied [99]. The efficiency of the electron emission has been significantly improved by oxidizing PS using a rapid thermal oxidation (RTO) procedure [99]. Further improvements of the surface-emitting cold cathodes based on PS diodes have been achieved using a multilayered PS structure [100] and a multilayered graded PS structure [101], in addition to the RTO process.

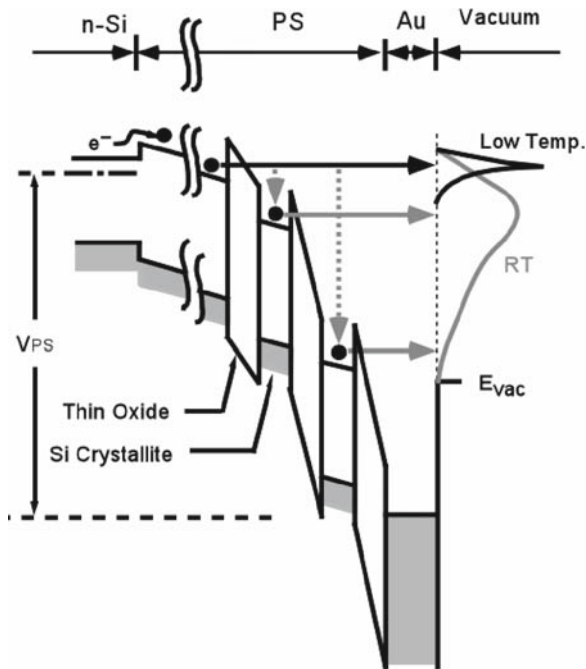


FIG. 7. Band diagram illustrating the generation and emission processes of quasi-ballistic electrons in porous Si diodes under biased condition. The curve in the vacuum part of the diagram shows the shape of the energy-dependence of the electron emission at room temperature and at 100 K. The narrowing of the curve at low temperature is attributed to significant reduction of thermal scattering in PS [111].

Another noticeable characteristic of graded-multilayered structures is the voltage tunability of the energy of emitted electrons. This indicates that there is little serial scattering loss during drift in PS. On the contrary, when using normal or multilayered structures, this voltage tunability of the emitted electron energy is not observed, suggesting that electrons are thermalized after serial scattering losses due to possible potential fluctuations.

The dynamics of electron emission is limited by the capacitance of PS. It depends on the surface of the emitter. The response time of a device with a 0.2 cm^2 surface is in the microsecond range.

3.3. Ballistic Electron Surface-Emitting Display on Glass Substrate

Electron emission has been obtained with porous poly Si (PPS), using the graded-multilayered structure [102]. $1.5\text{-}\mu\text{m}$ thick poly Si film was deposited onto an n^+ type Si wafer by low-pressure chemical vapor deposition. Efficiency of 1% was reached above 15 V. Over $200 \mu\text{A cm}^{-2}$ was obtained at 30 V. The stability of I_e and I_{PS} were very good. 4×4 pixels prototype display panel was then demonstrated [103, 104].

The group of Prof. Koshida, in collaboration with Japanese companies, has developed a ballistic electron surface-emitting display on a glass substrate using a

low temperature process [105]. The flat panel display was $168 (\text{RGB}) \times 126$ pixels, 2.6 in. diagonal full-color. Subpixel size was $320 \times 107 \mu\text{m}$. Since RTO requires very high temperature for the glass substrate, a low-temperature process, the ECO technique, which was proposed by Gelloz to enhance the PS EL characteristics [4, 58], was used. The device could operate at relatively low vacuum level (10 Pa) and without any focusing electrodes even when the distance between pixels was only $40 \mu\text{m}$. The same group then reported a prototype of a larger display (7.6 in. in diagonal) [112].

3.4. Solid-State Planar Luminescent Devices

A principle of planar-type visible light emission has been reported using ballistic electrons as excitation source [113–116]. Both poly Si [113] and c-Si [114, 115] have been used. For the PS oxidation process, both RTO and ECO were used. The device is composed of a surface emitting cold cathode and a luminescent material directly deposited onto the electron emitter, as illustrated in the inset of Fig. 8 in the case of c-Si [114]. In this case, tris(8-hydroxyquinoline) aluminum (Alq_3) is used as fluorescent film, resulting in green EL emission. Any type of luminescent material could be used in order to produce any colors. Red and blue emission from organic compounds have also been demonstrated using DCM (4-(dicyanomethylene)-2-methyl-6-(4-dimethyl-aminostyryl)-4H-pyran) and TPB (1,1,4,4-tetraphenyl-1,3-butadiene), respectively [116]. The important point is that there is no need for a vacuum spacing between the cold cathode and the fluorescent material. Electrons injected into the nc-PS layer are accelerated via multiple tunneling through

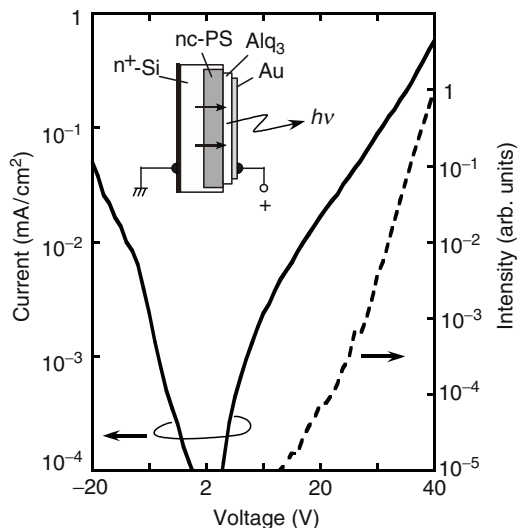


FIG. 8. Diode current and luminescence intensity as a function of voltage for the device shown in the inset. Reprinted with permission from [114] © 2002 American Institute of Physics [DOI: 10.1063/1.1508165].

interconnected silicon nanocrystallites, and reach the outer surface as energetic hot or quasiballistic electrons. They directly excite the fluorescent film, and then induce uniform visible luminescence.

Figure 8 also shows the current density and the EL intensity as a function of the voltage [114]. No EL could be recorded under reverse operation since no electrons could be emitted under this condition. The EL spectrum was the same as the PL one, showing that the light emission comes from Alq_3 . The superlinear behavior of the EL intensity vs. current density relates to the voltage-controlled characteristic property of this device. Indeed, as the driving current is increased, the relative number of energetic emitted electrons is significantly enhanced.

A device in which the luminescent layer is also PS has been investigated [117]. The two types of nc-Si layers were sequentially formed by electrochemical anodization under appropriate conditions. When a positive bias voltage is applied to the top electrode, electrons injected into the bottom nc-Si layer from the substrate are accelerated toward the outer surface, excite the luminescent nc-Si layer to generate electron-hole pairs, and induce visible luminescence through their radiative recombination. The intrinsic EL of the nc-Si diode was significantly enhanced by the introduction of the ballistic excitation mode.

4. SI NANOCRYSTALS SURROUNDED BY SI OXIDE

EL from Si nanostructures has been observed in various systems, in addition to PS. One of the most studied configuration is Si-rich SiO_2 . It is also important since light amplification in such systems has been reported [118]. The characteristics of a selection of devices discussed in this section can be found in Table 6.

4.1. Fabrication, Photoluminescence, and Introduction to EL

The excess of Si in SiO_2 can be generated either during SiO_x deposition (usually by CVD or sputtering) and further separation of the Si and SiO_2 phases by annealing [119–122], or by Si implantation in SiO_2 [123–126] and subsequent annealing in order to (1) fix damages induced by the implantation process and (2) agglomerate Si ions in clusters. The annealing process agglomerates the ions in clusters with different effectiveness depending on the temperature and time. Although low-temperature annealing eliminates most structural defects, the oxygen deficiency defects (believed to be at the origin of the UV and blue emission) are stable up to about 1,100°C. Higher temperature annealing favors the formation of clusters emitting red light originating from quantum confinement. In general, this approach leads to large Si nanocrystal size distribution but rather good surface passivation and layer mechanical strength. The main problem of these structures is difficult carrier injection since the host matrix is usually an insulator. The degree of interconnection of the Si nanocrystals is important and can be adjusted by the preparation conditions in order to increase the film conductivity. However, a high degree of interconnection also induces a weaker PL efficiency due to exciton migration to nearby Si nanocrystals, some of which may not be luminescent [126].

Table 6 Some characteristics of most devices discussed in Sect. 4, about LEDs based on Si-rich SiO₂

Structure	nc-Si synthesis	Injection	Voltage, Current	EL peak, λ	Speed	Efficiency	Stability	Year	Ref.
Si(p)/Si-rich SiO ₂ /Au	Sputtering; annealing	Bipolar injection	>4 V	650 nm	–	–	–	1995	[139]
Al/Si(p)/SiO ₂ + nc-Si/Au	Si ⁺ implantation; annealing	–	5–15 V; 25–200 mA	600 nm	–	–	–	1997	[132]
Si(p)/SiO ₂ + nc-Si/poly-Si (n)	Si ⁺ implantation; annealing	Impact excitation	>8 V	800 nm	–	EQE < 0.02%	Very stable	1999	[134]
Si(n)/SiO ₂ + nc-Si/ITO	Sol-gel; Si ⁺ implantation; annealing	Bipolar injection	>5 V; >1 A cm ⁻²	750 nm	–	EQE = 10 ⁻⁵ %	2000	[133]	
Al/Si(p)/SiO ₂ /nc-Si (single layer)/SiO ₂ /Al	CVD; thermal oxidation	–	5–10 V; <10 mA	Voltage-tunable: 800 nm–600 nm	–	–	–	2000	[147]
Si(p ⁺)/SiO ₂ + nc-Si/Metal	CVD; annealing	Impact excitation	4 V; 0.2 mA cm ⁻²	900 nm	<40 kHz	–	–	2002–2003–2004	[140–143]
Si(p)/SiO ₂ + nc-Si/Al	Si ⁺ implantation; annealing	Bipolar injection (hopping)	<5 V	800 nm	–	–	Stable	2003	[136, 137]
Si(p)/SiO ₂ + nc-Si/poly-Si (n)	Si ⁺ implantation; annealing	Impact excitation	5–14 V	800 nm	–	QE = 19% (single nc-Si)	Very stable	2004	[131]
EL of single nc-Si									
Si(p)/SiO ₂ + doped nc-Si/Au	Si ⁺ , P ⁺ , B ⁺ implantation; annealing	Impact excitation	–	~730 nm	–	–	–	2005	[135]
nc-Si floating-gate transistor	MOS techniques	Programmed sequential bipolar injection by F–N tunneling	6 V	750 nm	10 kHz	–	Stable	2005	[148]
Al/Si(n)/Si-rich SiO ₂ /Ag	Si ⁺ implantation; annealing	Hopping + Impact excitation	3.3 V; 0.15 A cm ⁻²	White	–	–	–	2005	[138]
Al/Si(n)/Si-rich SiO ₂ /Ag	SiO _x CVD annealing	Bipolar injection by tunneling	>86 V; >215 μ A cm ⁻²	760 nm	–	–	–	2005	[138]

EQE External quantum efficiency. Stated voltage and current are the minimum values for EL detection, or the device operation conditions

The PL external QE efficiency of these structures was typically quite low (about 0.1–0.3%) until recently, when Wang et al. [1] reported an external QE of 12%. The trick used by the authors to get such a high value is to set the substrate temperature to RT during the film deposition, instead of heating it to above 200°C as usually accepted in PECVD. As a result, the Si nanocrystals were nearly strain-free and the Si–SiO₂ interface was sharp. The quality of the interface between the Si nanocrystals and the surrounding matrix is indeed critical to get high luminescence efficiencies. This fact is also illustrated by the very high PL external QE (23%) obtained by Gelloz et al. [2, 3] in PS using HWA (see Sect. 2.6).

In addition to the passivation role, the oxide surrounding the Si nanocrystals also plays a major role in the luminescence via interface states. On one hand, this is a major problem when one wants to obtain blue emission from the Si nanocrystals themselves since levels inside the gap induce red emission instead of blue [11]. On the other hand, these levels could be extremely important and desirable since they may be crucial to the observation of optical gain [118].

The PL [127–130] and EL [131] of single Si nanocrystals surrounded by SiO₂ have been studied. The best PL quantum efficiency reached 35% (19% for the EL), which is encouraging for the application in EL devices. However, the blinking, and the long radiative lifetime (0.1 ms), consequence of the indirect band-gap structure, could be a major limitation for interconnect purposes, though display applications could still be considered.

The EL introduces an addition challenge: efficient injection of the charge carriers into Si nanocrystals. Electron–hole pairs are usually generated either by bipolar injection from both electrodes of the diode or by impact excitation. In the latter case, only electrons flow through the device and holes are generated by impact processes.

4.2. Si-Implanted Si Oxide

The approach consisting in Si implantation in a matrix such as SiO₂ has lead to several reports. Among these, Song et al. [132] have studied the EL of Si⁺ implanted thermally formed SiO₂. The oxide layer was 34 nm thick. Si was implanted (25 keV, 10¹⁶ cm⁻²) mainly in the bottom half of the oxide layer. Both PL and EL show three bands, around 470, 600, and 730 nm. However, the 600-nm band is the strongest in EL whereas it is weaker in PL. The relative contributions from different luminescence bands to EL depend on the annealing conditions. From the study of different annealing conditions, the authors conclude that the 470-nm band needs too high excitation energy to be electrically excitable. The 730-nm band depends on the existence of Si nanocrystals, which are not numerously produced until high temperature annealing. The 600-nm band is easy to excite electrically due to its low energy. Moreover, the presence of Si nanocrystals improves the EL from oxygen-related defects.

Luterova et al. [133] have observed red EL from Si⁺-implanted sol–gel-derived SiO₂ films on n-type Si. The oxide layer was 250 nm thick. Four different energies and ion doses have been used for the Si implantation in order to get a flat ion profile

across the oxide layer. Annealing was performed at 1,100°C for 1 h. EL was observed from 5 V and 1 A cm⁻². The device showed no rectifying behavior but the EL could be obtained only at one bias polarity. EL at 295 K was emitted only from a small number of bright spots. The EL spectrum showed only a peak at 750 nm (attributed to Si nanocrystals) whereas the PL showed the same peak plus another one in the blue range attributed to the presence of defects. The EL was attributed to electron–hole recombination in Si nanocrystals as a result of carrier injection. Si nanocrystals are believed to create several conductive percolation paths across the oxide layer. The low efficiency (10⁻⁵%) was attributed to shunting current paths due to defects. The EL decay is 8 μs.

Lalic et al. [134] have studied the fabrication and the electroluminescent properties of Si nanocrystals in SiO₂. The Si nanocrystals were generated by ion implantation and further annealing at 1,100°C for 1 h. Both the Si dose and SiO₂ thickness have been varied. The oxide thickness has been varied from 12 to 100 nm. The thermal oxide was grown on a p-type Si substrate. Then a 210-nm thick a-Si layer was deposited for use as a protective and contacting layer as well as to adjust the position of the implantation profile peak. A 160-nm thick highly phosphorous-doped poly-Si layer was then deposited and used to enhance the carrier injection into the Si nanocrystals. EL was observed from LEDs with oxide thickness less than 18 nm for bias voltages above 8 V. The EL spectrum shows a peak at about 1.55 eV. The EL efficiency is found more than one order of magnitude lower than that of their previously reported LED based on PS [42–44], which should be less than 2 × 10⁻²%. However, the EL of the new device shows no degradation (due to Si nanocrystal passivation by SiO₂). This is very much better than the results they obtained with PS. Higher implantation doses lead to a higher level of interconnection between Si nanocrystals. More interconnected structures induce shorter EL time constants, larger leakage currents, and lower efficiency. The same group has studied the PL [127–130] and EL [131] of single Si nanocrystals in the same kind of devices. The EL was observed at voltages above 5 V. Its mechanism was impact excitation of electron–hole pairs in Si nanocrystals. The EL was stable and visible by naked eye. The best EL quantum efficiency was 19% for a single quantum dot.

The effect of boron or phosphorous dopant incorporation in the structure has been studied [135]. Si⁺, P⁺, or B⁺ were implanted into p-type thermally oxidized Si. The samples were then annealed at 1,000–1,100°C. The EL was excited by impact by hot electrons. It was always improved by the doping, up to ten times.

For many devices in this category, the injection mechanism is impact excitation. However, this mechanism leads to device degradation upon prolonged operation. The ideal injection scheme would involve bipolar injection from both electrodes of the diode. Such injection mechanism has been realized using a p⁺-Si/SiO₂ + nc-Si/Al device structure [136, 137]. Forty nanometers of thick SiO₂ layers were twice Si-implanted in order to obtain a planar profile of the excess Si nanocrystals in the oxide. The SiO₂ layers were then etched at different depth, from 10 to 30 nm. Finally the samples were annealed at 1,110°C. The current was found not thermally activated and the Fowler–Nordheim regime was not observed for electric fields below 5 MV cm⁻¹. The transport mechanism was described as hopping, with

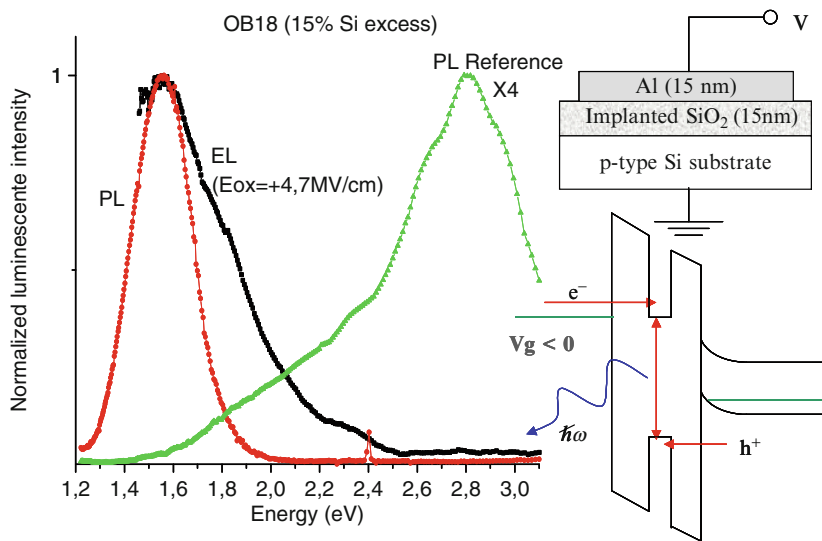


FIG. 9. PL and EL spectra for 15-nm thick implanted-oxide LED. The PL of a nonimplanted sample is shown for comparison. Reprinted from [137] © (2002) with permission from Elsevier.

an average trap distance between 1.4 and 1.9 nm. Figure 9 shows a schematic representation of the device, the EL model, and spectra of EL and PL. Stable red EL was observed at RT. Since the EL and PL exhibit the same energy peak, they relate to the same origin, recombination of carriers trapped by the surface states of the Si nanocrystals. The higher energy part of the EL spectrum was attributed to SiO_2 radiative defects.

Very recently, Lin et al. [138] studied the effect of the defects in SiO_x on the EL characteristics. They built two devices, both consisting in $\text{Al/n-Si/SiO}_2 + \text{nc-Si/Ag}$ structure. One included a multienergy Si-implanted SiO_2 layer, whereas the other one included a substoichiometric SiO_x layer. Both layers were annealed. The Si-implanted layer was including many defects which induced blue and green EL bands in addition to the conventional red band due to Si nanocrystals, leading to white EL. In this device, the threshold voltage, current, and electric field were 3.3 V, 0.15 A cm^{-2} , and 66 kV cm^{-1} , respectively. The transport mechanism was attributed in part to hopping and enhanced Fowler–Nordheim tunneling, and the EL mechanism to carrier injection and impact excitation of different defects in the oxide layer. The EL was only observed under reverse bias. Maximum optical output was 120 nW at 15 V. The device including the annealed SiO_x layer exhibited a much higher voltage threshold (86 V) than the previous device. This was attributed to fewer nonradiative and irradiated defects within the PECVD-grown Si-rich SiO_x material. The carriers in nc-Si were neither thermally activated nor field-enhanced Fowler–Nordheim tunneling injected, but possibly assisted by direct tunneling between Si nanocrystals. The device was emitting near-infrared light (600–800 nm).

4.3. Annealed Substoichiometric Si Oxide

Qin et al. [139] have studied the visible EL from Au/extra thin Si-rich SiO_2 /p-type Si structures. The oxide thickness was 4 nm. It was grown by magnetron sputtering. The EL was observed at voltage above 4 V. The EL showed a peak at 1.9 eV with a FWHM of 0.5 eV when the Si-rich oxide film was not annealed. Annealing at 800°C induces a widening of the EL spectrum and the appearance of several shoulders at about 1.5, 2.2, and 2.4 eV. Furthermore, the EL peak energy blue shifts with increasing forward bias. The luminescence is believed to originate from several types of luminescent centers in the Si-rich Si oxide film.

One group has produced several reports recently showing promising results of EL from Si quantum dots embedded in the oxide of MOS structures [140–143]. A 25-nm thick substoichiometric SiO_x ($x < 2$) film was deposited on a p⁺-type Si substrate by PE-CVD and annealed at 1,100°C for 1 h in N_2 in order to induce separation of the Si and SiO_2 phases. The Si nanocrystals thus formed had a mean radius of about 1.0 nm. The excitation cross section of Si nanocrystals under electrical pumping ($4.7 \times 10^{-14} \text{ cm}^2$) was found two orders of magnitude higher than under optical pumping [140]. This was also the case for Er excitation in their similar device including implanted Er ions [144]. The mechanism responsible for the light emission was the same under both optical and electrical pumping (self-trapped exciton recombination at a Si=O interfacial state). The charge carrier transport was Fowler–Nordheim tunneling and the injection mechanism was attributed to impact processes. Efficient EL was obtained at 4 V and 0.2 mA cm^{-2} . The EL spectrum exhibited a peak at about 900 nm. EL response time could be lowered down to about 25 μs [140]. The effect of the Si concentration in the SiO_x layer was studied [143]. Figure 10 (Fig. 4) shows the EL intensity as a function of voltage for devices based on active layers with different Si concentrations. It shows that the threshold for light emission increases by decreasing the Si concentration in the SiO_x film. These devices are very stable.

4.4. nc-Si Single Layer Sandwiched Between Two SiO_2 Layers

Devices including a few nanometer thick amorphous Si layer sandwiched between two SiO_2 layers have been investigated [145, 146]. A forward bias p-type Si/ SiO_2 /a-Si/ SiO_2 /Au [145] and a reverse biased n⁺-type Si/ SiO_2 /a-Si/ SiO_2 /Au [146] have been studied. The thickness of the a-Si layer has been varied between 0 and 4 nm. The upper and lower SiO_2 thicknesses were 3.0 and 1.5 nm, respectively. Room temperature EL is observed at about 5–7 V in the wavelength range from 600 to 700 nm depending on a-Si thickness. In both devices, EL peak intensity and peak wavelength synchronously swing with increasing the a-Si layer thickness [145]. The swing period is consistent with half the de Broglie wavelength of the carriers [146]. The EL is mainly attributed to luminescent centers in the oxide (excited by electrical breakdown), with a minor contribution of the a-Si layer as a result of quantum confinement.

Photopoulos et al. [147] studied room- and low-temperature EL in the visible from a single layer of Si nanocrystals in between two thin (5 nm) SiO_2 layers. The

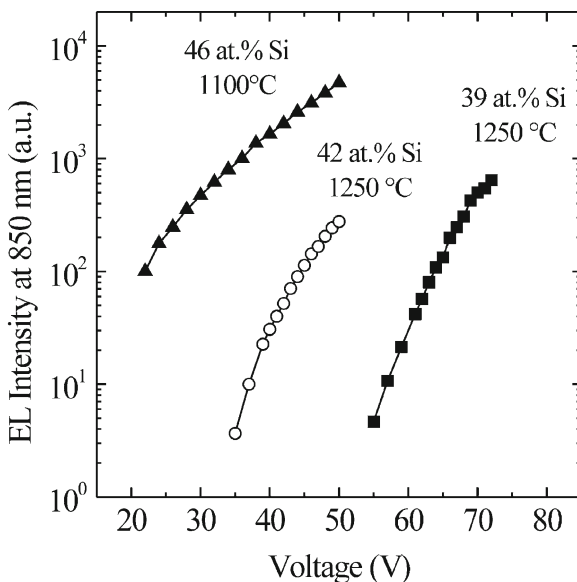


FIG. 10. EL intensity at 850nm as a function of the applied voltage under forward bias conditions for devices characterized by different active layers. Reprinted from [143] © (2004) with permission from Elsevier.

EL was attributed to quantum confinement. The effects of size and size distribution were demonstrated. The EL peak wavelength exhibited a voltage-tunability from the red (800nm) to the yellow (600nm). The authors suggest different possible mechanism to explain the voltage tunability of the peak wavelength: selective carrier injection in Si nanocrystals of different sizes, an enhanced Auger recombination rate at high voltages, Coulomb charging, and quantum-confined Stark effect.

A new device operation has been proposed recently: field-effect light emission using a floating-gate transistor structure [148]. The gate oxide was the host of the Si nanocrystals. Figure 11 shows the device structure as well as the device operation mechanism. Electrons and holes tunnel sequentially from the channel under the influence of an alternating voltage applied to its gate (6 V). The sequential accumulation of electrons and then holes within the Si nanocrystals on each cycle thereby results in recombination and the emission of light (broad spectrum centered at 750nm in the report of Walters et al. [148]). This injection scheme presents several advantages compared to the conventional diode structure. The field necessary to produce light is small compared to that in diodes because the carrier tunneling efficiency is governed only by the distance between the nanocrystals and the channel and not by their density or the total matrix thickness. In addition, the degradation of the oxide due to impact processes should be avoided, leading to long life operation. The device of Walters et al. [148] was indeed very stable. Finally, the fabrication techniques are that of conventional electronics, and thus fully compatible with VLSI. There is one negative point that still remains though. The speed of the device is still limited by the long luminescence lifetime of the Si nanocrystals (tens of

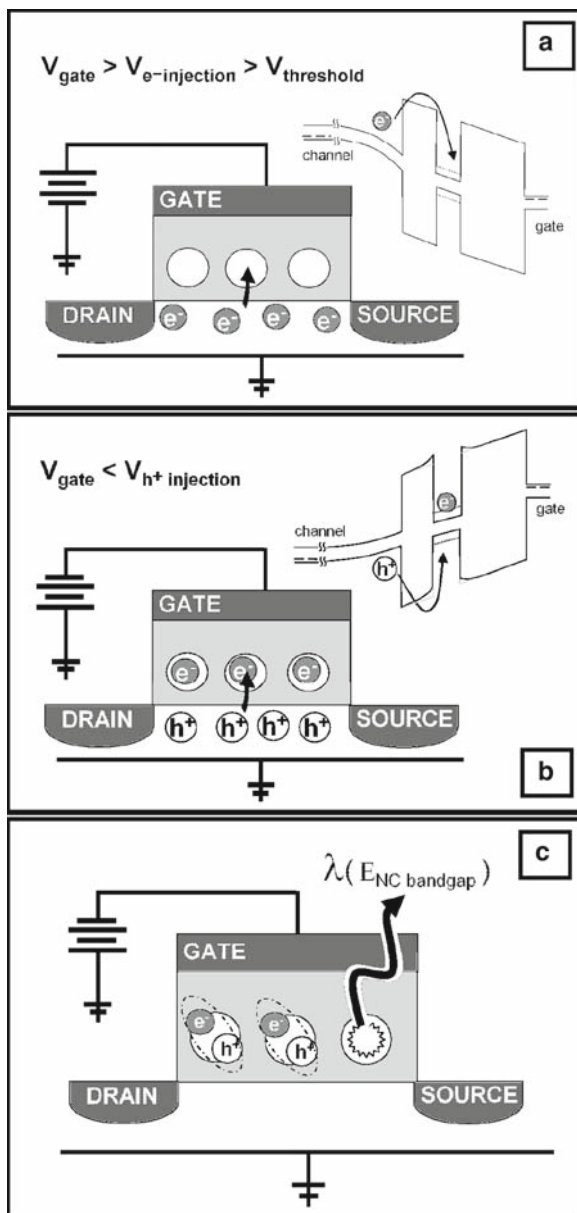


FIG. 11. Schematic of the field-effect EL mechanism in a Si nanocrystal floating-gate transistor structure. *Inset band diagrams* depict the relevant tunneling processes. (a–c), The array of Si nanocrystals embedded in the gate oxide of the transistor can be sequentially charged with electrons (a) by Fowler–Nordheim tunneling, and holes (b) via Coulomb field-enhanced Fowler–Nordheim tunneling to prepare excitons that radiatively recombine (c) [148]. Reprinted by permission from Macmillan Publishers Ltd, © (2005).

microseconds) due to their indirect bandgap. As a result, the potential application remains in the display arena rather than interconnects.

5 OTHER SINGLE LAYER NANOSTRUCTURES

The characteristics of a selection of devices discussed in this section can be found in Table 7.

5.1 *nc-Si Embedded in SiN_x*

Park et al. [149] have used a silicon nitride film as the host matrix for Si nanodots. Amorphous Si quantum dots were formed in SiN_x by PE-CVD. Control of dot size led to red, green, and blue PL. An orange LED was fabricated using Si dots with a mean size of 2.0 nm. The turn-on voltage was below 5 V. The EQE was about $2 \times 10^{-3}\%$.

A device also based on Si nanocrystals embedded in a SiN_x matrix exhibited a relatively high external QE (1.6%) [5]. This is currently the highest value reported to date for a light-emitting device based on nanocrystalline Si. It is greater than the 1.1% that was earlier reported by Gelloz et al. [4] with a device based on PS. Figure 12 shows a schematic representation of the device as well as the evolution of the current density as a function of the voltage. The solid curve is a fit of the data using a Fowler–Nordheim equation. The EL was orange and was observed at current greater than 1 mA. An emitted power of 2 mW was obtained for a current of 70 mA. The n-type SiC semitransparent layer is crucial to inject electrons while allowing the EL to exit the device.

Another configuration has been investigated by Chen et al. [150]. nc-Si/a-SiN_x was grown by e-beam evaporation of Si into an inductively coupled plasma of nitrogen. Holes were injected by an ITO electrode whereas electrons were injected by an Ag electrode in one case or a Ca/Ag electrode in another case. The second configuration showed better results. It outperformed the configuration with a simple Ag electrode by increasing the current density, the maximal luminance, and the EL efficiency of the device. The turn-on voltage was 10 V, and the EL efficiency 0.16 Cd A^{-1} . A maximum of 0.25 Cd m^{-2} was obtained, at 12 V.

5.2 *Other Low-Dimensional Si Structures*

EL from Si nanopillars has been reported by Nassiopoulou et al. [151, 152]. Si nanopillars were fabricated by using deep UV lithography, highly anisotropic Si reactive ion etching, and high-temperature thermal oxidation for further thinning. The pillars (lying on and perpendicular to, the original Si substrate) were below 10 nm in diameter and 0.4–0.6 μm high. The space between pillars was filled with an isolating transparent polymer. The top contact was either gold or ITO. Weak and low efficiency EL peaking at about 675 nm was observed at voltages above 12–14 V. EL was stable for several hours [152].

The potential of visible EL from Si nanocrystals embedded in a-Si:H film has also been investigated. Tong et al. [153] produced such electroluminescent layers by

Table 7 Some characteristics of most devices discussed in Sect. V, about LEDs based on various types of nanostructures excluding Si-rich SiO₂

Structure	Nanostructure	Injection mechanism	Voltage, Current	EL peak, λ	Speed	Efficiency	Stability	Year	Ref.
Si(n)/nc-Si/Au	CVD	Bipolar injection	6–22 V	630 nm and 730 nm	–	–	–	1996	[153]
Si(n)/Si nano-pillars/ITO	Lithography; etching	–	10–40 V	650 nm	–	–	Hours	1996	[151, 152]
Si(p)/nc-Si/Pt	Laser ablation; annealing	Impact excitation	7–30 V; 1–20 mA	770 nm	–	EQE = 10 ⁻⁴ %	–	1997	[155]
Glass/SnO ₂ /nc-Si(p)/Al	CVD; anodization	Bipolar injection	5–10 V	790 nm	–	EQE < 0.01%	–	1998	[158]
Ti-Au/Si(p ⁺)/a-Si + nc-Si/Ti-Au	a-Si deposition; annealing	Impact excitation	4.5 V; 60 mA	650 nm	–	–	–	1999	[154]
AuSb/Si(n)/Si(p ⁺)/Al	B implantation	Bipolar injection	>0.7 V; >1 mA	1,150 nm	25 kHz	EQE = 0.02%	–	2001	[160]
Si(p)/SiN _x + nc-Si/Ni/Au	CVD	–	5–10 V; <500 mA cm ⁻²	Red, green, or blue	–	QE = 0.1% EQE = 0.002%	–	2001	[149]
Si(p)/SiN _x + nc-Si/NiO	–	–	–	–	–	–	–	2001	[156, 157]
Pt/Si(p)/In ₂ O ₃ + nc-Si/ITO	Laser ablation; annealing	Impact excitation	–	1,060 nm or red and blue	–	–	–	2001	[156, 157]
Si(p)/SiO ₂ -doped Si/Metal	Sputtering	Bipolar injection	7–10 V; 50–500 mA	1,400 nm	–	–	–	2002	[159]
In/Si(n)/nano-structured Si(p ⁺)/In	Spin-on doping; SiO ₂ nanoparticles; thermal diffusion	Bipolar injection	200–600 mA	1,155 nm	–	IQE = 0.1%	–	2004	[163]
Stimulated emission in ridge waveguide							EQE = 0.013% in ridge waveguide		
n ⁺ p diode	B or P implantation	Bipolar injection	<1.5 V	1,170 nm	–	IQE = 2%	–	2005	[161]
Ca-Ag/a-SiN _x + nc-Si/ITO	e-beam/plasma	Bipolar injection by tunneling	>10 V; >100 mA cm ⁻²	440–500 nm	–	0.16 Cd A ⁻¹	–	2005	[150]
Si(p)/SiNx + nc-Si / SiC(n)/ITO	CVD annealing	Bipolar injection by F–N tunneling	3–20 V; 0.18–12.7 mA cm ⁻²	600 nm	–	EQE = 1.6%	–	2005	[5]

EQE External quantum efficiency and *IQE* internal quantum efficiency. Stated voltage and current are the minimum values for EL detection, or the device operation conditions

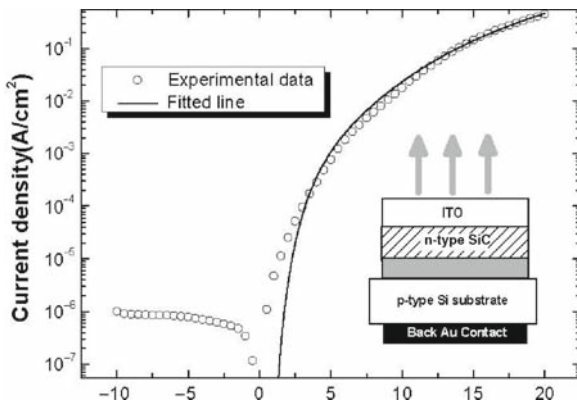


FIG. 12. Current density vs. applied voltage. Open circles and solid line denote the experimental data and the fitted data, respectively. The experimental data are best fitted by the expression for the Fowler–Nordheim tunneling process. The *inset* shows the schematic of the device. Reprinted with permission from [5] © 2005 American Institute of Physics [DOI: 10.1063/1.1866638].

CVD. The EL spectrum showed two peaks, at about 630–680 nm and 730 nm. EL detection threshold was about 6 V. This value increased when the film conductivity decreased. In addition, the EL intensity increased with the film conductivity. The EL mechanism was not clear. Fujita et al. [154] used an ultrathin a-Si layer containing Si nanocrystals. The device was a TiAu/p⁺-Si/a-Si + ncSi/TiAu structure. Orange EL could be seen at RT with the naked eye under reverse applied voltages of about 4.0–4.5 V. The EL spectrum included a major peak at 1.9 eV and a minor peak at 2.2 eV. The EL excitation mechanism was attributed to an impact process.

One group has investigated the EL from Si nanocrystals prepared by laser ablation [155–157]. In the report of Yoshida et al. [155], the diode structure was Pt/closely packed Si nanocrystals/p-type Si/Pt. EL at 1.66 eV at room temperature was obtained. The EL energy peak was lower than the PL one (2.07 eV). The EL current and voltage threshold (photomultiplier detection) were 1 mA and 7 V, respectively. Detection threshold by the naked eye in the dark were 15 mA and 25 V for the current and voltage, respectively. The active area was 0.031 cm². The estimated external QE was 10^{−4}%. A strong superlinear dependence of the EL intensity on the current density was attributed to the EL generation mechanism, namely impact ionization by minority hot carriers. The effects of annealing on the structure and the optical properties of the luminescent layers were later reported [156]. A number of new emission bands appeared, which was explained by the enhanced crystallinity after annealing in N₂. Annealing in O₂ led to the appearance of a blue EL band attributed to luminescence of neutral oxygen vacancy defects in SiO₂. The same group also studied the effect of an In₂O₃ passivating layer on top of the nc-Si layer [157]. When this layer was deposited without breaking the vacuum, the EL spectrum had a narrow bandwidth of 0.15 eV peaked at 1.17 eV at RT. However, when the nc-Si layer was exposed to air before In₂O₃ deposition, a broad EL spectrum was obtained

(peak: 1.7 eV, bandwidth: 0.46 eV). The visible emission was attributed to various oxide-related emission centers.

Toyama et al. [158] have observed EL from a glass/SnO₂/p-type Si nanocrystals/Al structure by applying positive bias voltage to the SnO₂ electrode. P-type Si nanocrystals were first deposited onto SnO₂-coated glass by PE-CVD. This Si layer is then anodized in HF. This anodization is likely to lead to a porous amorphous Si layer. Si nanocrystals sizes were estimated to be in the range of 3–5 nm. The EL showed a peak at 1.57 eV. The EL onset voltage was about 5 V. The EQE was below 10⁻²%. The EL was attributed to radiative recombination of electrons injected from the Al electrode and holes in the p-type Si nanocrystal film. The authors suggested that electron injection was a result of a tunneling process at the interface of Si nanocrystals/Al.

Osaka et al. [159] reported EL at 1,400 nm from a p-type Si/SiO₂-doped Si/Metal diode. SiO₂-doped Si was deposited by RF magnetron sputtering technique on p-type Si at a substrate temperature of 400°C. The EL was attributed to hole injection from the substrate followed by optical transition between electron-bound states in the film and injected holes. The EL spectrum was much narrower (FWHM 125 nm) than the PL one (FWHM 400 nm). This behavior was attributed to the hole density of states being much broader than the electron-bound state distribution. The films showed optical absorption in the range 1.4–2.0 eV, comparable to that of undoped a-Si:H films. The SiO₂-doped Si films may be useful for photovoltaic applications.

5.3. Confinement Induced by Local Strain or Doping Fluctuations

Ng et al. [160] fabricated a device in which the non radiative recombination rate in bulk silicon is reduced as a result of carrier localization. Carrier localization is achieved by a three-dimensional local strain field induced by appropriately produced dislocation loops in the pn junction. These dislocation loops as well as the p part of the junction are produced in two simple steps: boron implantation at a dose of $1 \times 10^{15} \text{ cm}^{-2}$ at an energy of 30 keV, and subsequent annealing in nitrogen atmosphere for 20 min at 1,000°C. The dislocation loops form an array situated in a planar region parallel to, and around 100 nm from, the pn junction. They are about 80–100 nm in diameter and are spaced around 20 nm apart. These loops are said to induce a blocking potential that confines carriers close to the junction region. At 100 mA forward current, the emitted light was 19.8 μW and the external QE was about $2 \times 10^{-2}\%$ at room temperature. The device response at room temperature was about 18 μs . At room temperature, the emission spectrum shows a peak at around 1,150 nm. This type of diodes has been studied by other research groups. An internal QE of 2% was reported at 300 K by Kittler et al. [161], whereas an external power efficiency of 0.12% was reached by Sun et al. [162]. An interesting feature of these diodes is that the EL and PL efficiencies increase with the temperature. This unusual property has been explained by thermal activation of carrier from bound excitons having low recombination rates [161, 162].

Enhanced EL from bulk Si p⁺n junctions has also been obtained by Chen et al. [163] by using spatial confinement of carriers induced by doping fluctuations. The

carrier localization nanostructure was made using nonuniform diffusion of dopant though SiO_2 nanoparticles. EL peaked at 1,150 nm was measured at RT, with a maximum internal QE of about 0.1%. The incorporation of the pn junction into a ridge waveguide led to stimulated emission at 1,214 and 1,217 nm. The different emission wavelengths were attributed to the free and bound excitons.

6. SUPERLATTICES

Most devices discussed in this section have their main properties listed in Table 8.

6.1. Superlattices Based on SiO_x Layers

The first LEDs based on Si– SiO_2 superlattices were fabricated by molecular beam epitaxy [164]. The basic period of the superlattice was formed by a monolayer of adsorbed oxygen and a thin deposited single crystal Si layer. Both EL and PL were observed. The luminescence was attributed to quantum confinement as well as Si/O binding regions. The EL was stable for more than a year.

Poly-Si/ SiO_2 superlattices were formed by PE-CVD [165, 166]. The thickness of the Si layer was varied either from 1 to 3 nm (up to 60 periods) or from 75 to 150 nm (up to 4 periods) [165]. The oxide layer was around 1 or 2 nm. All structures were containing Si nanodots. At low current injection, the emission was red and the quantum efficiency was low (about $10^{-3}\%$). The author latter suggested that this EL originates from defect levels on the oxide near the interface [166]. At larger injection current, the EL intensity was superlinear with respect to the current density and a blue shift occurred together with a narrowing of the FWHM down to about 5 nm. These phenomena are consistent with plasma emission in the intergrain regions.

Nanocrystalline Si/ SiO_2 superlattices have been fabricated by alternate sequences of LP-CVD of thin Si layers and high temperature thermal oxidation [167]. The initially amorphous Si films were crystallized during the oxidation step used to make to top oxide layer. Multilayers with five or ten periods were fabricated, with nc-Si thickness between 1.5 and 5 nm, and SiO_2 thickness between 5 and 101 nm. The EL spectrum showed several peaks at 550, 650, and 750 nm.

Gaburro et al. [168] have also fabricated light-emitting Si/ SiO_2 superlattices by LP-CVD. The Si and SiO_2 thicknesses were 2 and 5 nm, respectively. The fabrication process was CMOS compatible. The PL band shows a peak at 800 nm due to quantum confinement, whereas the EL shows two bands. One band in the infrared region was attributed to blackbody radiation. The other band was visible and was attributed to coupling of energetic electrons with surface plasmon-polaritons, or to hot-electron relaxation. EL was observed from 2 mA for a contact area of $5 \times 10^{-5} \text{ cm}^2$. The external QE was $2 \times 10^{-4}\%$. The same group also reported an external QE of $5 \times 10^{-3}\%$ [169].

Heng et al. [170] fabricated a LED based on an amorphous Si/ SiO_2 superlattice deposited on a p-type Si substrate, by sputtering. The thickness of the a-Si layers was varied in a range 1.0–3.2 nm. The thickness of the SiO_2 layer was 1.5 nm in all devices. EL was observed above about 5 V. Every EL spectrum could be decomposed

Table 8 Some characteristics of most devices discussed in Sect. 6, about LEDs based on superlattices

Superlattice structure	Main techniques	Injection mechanism	Voltage, Current	EL peak, λ	Speed	Efficiency	Stability	Year	Ref.
a-Si:H/a-SiN _x :H	CVD; laser heating	Bipolar injection	>7V	650 nm	–	Low	–	1999	[174]
Si/SiO ₂	CVD	Hot-electron relaxation	>7V	650 nm	>1 MHz	0.005%	Stable	1999	[169]
Si + CaF ₂ /CaF ₂	MBE; RTA	Bipolar injection	10V; 2 mA	White	–	–	–	1999	[180, 181]
								2000	
Si/SiO ₂	CVD	–	8V pulsed	550 nm; 650 nm; 750 nm	–	–	–	2000	[167]
Si/CaF ₂				700 nm				2000	[180]
a-Si/SiO ₂	Sputtering	Bipolar injection	>5V	680 nm; 560 nm	–	–	–	2001	[170]
		EL from centers in SiO ₂							
Poly-Si/SiO ₂	CVD	Bipolar injection	>5V	550–800 nm	–	–	–	2001	[166]
		EL from centers in SiO ₂	4 A cm ⁻²						
Si/CaF ₂	MBE	–	>4V	700 nm	–	–	Hours	2001	[182, 183]
			>100 mA cm ⁻²						
a-Si/SiO ₂	Sputtering	Bipolar injection by tunneling	5–11 V; 20–250 mA	650 nm	–	–	–	2001	[171]
				470 nm After gamma irradiation					
Si/SiO ₂	Sputtering	EL from centers in SiO ₂	12 V pulsed	620 nm	–	–	–	2002	[172]
SiO ₂ /SiO ₂ , EL at 80 K	e-Beam evaporation; annealing	–	2–4 V	Voltage tunable (950–725 nm)	–	Low	–	2005	[173]

Stated voltage and current are the minimum values for EL detection, or the device operation conditions

into two Gaussian bands with peak energies of 1.82 and 2.22 eV. The EL intensity and current swings synchronously with increasing the Si layer thickness with a period being consistent with half the De Broglie wavelength of the carriers. The authors had already observed the same behavior with using only a single period instead of a superlattice [145, 146]. They attribute the EL emission to defect centers rather than levels in quantum dots.

Ma [171] has studied the effects of gamma irradiation on the EL from Au/a-Si/SiO₂ superlattices/p-type structures. Different Si thicknesses were used. The EL peak was at 650 nm. After gamma irradiation, the EL peak intensity increased 2.5 times. Moreover, a new 470 nm blue peak emerged from the EL spectra. The EL was visible by naked eye. Its mechanism was attributed to the presence of luminescence centers in SiO₂ rather than to the Si nanostructure.

Averboukh et al. [172] have investigated Si/SiO₂ superlattices prepared by magnetron sputtering on p-type Si. Four periods were used (Si: 1.8 nm; SiO₂: 1.5 nm). The EL was excited by electrical pulses (12 V, 4 μ s). Both the PL and the EL had their peak at about 2.06 eV. The luminescence was attributed to transitions between localized defect states at the Si/SiO₂ interface.

Jambois et al. [173] have studied SiO/SiO₂ superlattices prepared by successive thermal evaporation of a SiO powder and evaporation of fused silica glass. The nc-Si size was controlled by the SiO thickness. The SiO₂ thickness was 5 nm whereas the SiO thickness was varied from 2 to 6 nm. A clear continuous shift in PL peak energy was observed as a function of the nc-Si size, from 1.5 eV for 6 nm size to 1.68 eV for 2 nm size. EL was observed at 80 K with a threshold voltage of 2 V. The EL increased as the

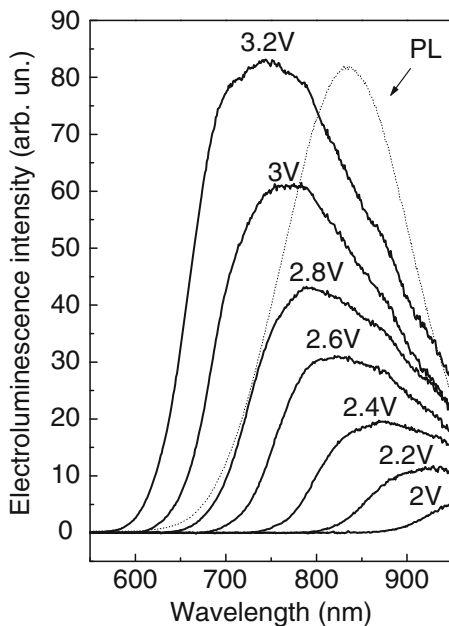


FIG. 13. EL spectra for a sample containing nc-Si with a mean size equal to 2.8 nm as a function of the bias voltage. The PL spectrum of the sample is represented in *dotted line*. Reprinted with permission from [173] © 2005 American Institute of Physics [DOI: 10.1063/1.2034087].

voltage was varied from 2 to 4 V, with a blue shift, as seen in Fig. 13. However, beyond 4 V, the EL intensity decreases and was not reproducible any more. The EL mechanism was attributed to both defects in SiO_2 and radiative recombination in nc-Si.

6.2. Superlattices Based on SiN_x or CaF_2 Layers

In addition to Si– SiO_2 superlattices, a-Si:H/a- SiN_x :H multi-quantum well structures have been studied for their EL properties [174]. The layers were deposited by PE-CVD, and subsequently annealed with an KrF excimer laser. The a- SiN_x :H layer was either 3 nm or 10 nm and the a-Si:H layer was varied from 2 to 4 nm. The LED structure was semitransparent electrode/crystallized a-Si:H/a- SiN_x :H multi-quantum wells/crystallized n^+ – a-Si:H/ SiO_2 /Si or quartz substrates. The EL spectrum showed multiple peaks around 600 and 700 nm. The onset of visible EL was 7 V in the best case. The EL mechanism was attributed to carrier injection into nanosized Si crystallites in the multi-quantum wells, and radiative recombination via Si quantum well states.

Another configuration, including CaF_2 /Si superlattices, has been investigated. PL [175–177] and EL [178–183] from these structures have been reported. A theoretical report attributes the EL emission from these structures to electron and hole tunneling through the CaF_2 barriers, occurring via Wentzel–Kramers–Brillouin mechanism [179]. Maruyama et al. [181] studied the EL of such superlattices on p-type Si. The superlattice was grown by molecular beam epitaxy and was followed by a rapid thermal annealing treatment. The EL was white. The EL spectrum is such that the emission increases from below 400 nm to more than 700 nm, whereas the PL has a peak at about 575 nm. The authors published some improvements 1 year later [180]. The electrical transport in these superlattices has been studied [183]. One hundred periods were used. The Si thickness was ranging from 1.2 to 1.6 nm, and the CaF_2 thickness was below 1 nm. At voltages higher than 4 V (both under forward and reverse conditions), a Poole–Frenkel-type mechanism accounted for the observed electric-field-assisted conduction through the layers. The same authors found that the EL spectra are slightly current tunable [182]. This was attributed to Auger quenching of the luminescence and size-dependent carrier injection.

7. EL FROM RARE EARTH-DOPED SI NANOCLUSTERS

The main properties of most devices discussed in this section can be found in Table 9.

The Er luminescence is greatly enhanced when incorporated into an SiO_2 matrix containing Si nanocrystals [184, 185]. Nonradiative de-excitation may be reduced due to enhanced localization. The emitting Er ions are located in the SiO_2 matrix or at the Si nanocrystal– SiO_2 interface [185]. The Si nanocrystals act as efficient sensitizers for the rare-earth ions. The coupling between Si nanocrystals and Er is indeed very strong. Transfer of excitation from Si nanocrystals to neighboring rare-earth ions is very effective.

Table 9 Some characteristics of most devices discussed in Sect. 7, about LEDs based on rare-earth doped Si nanostructures

Device structure	Ion incorporation	Injection mechanism	Voltage, Current	EL peak, λ	Speed	Efficiency	Stability	Year	Ref.
Al/Si(p)/Si-rich SiO ₂ :Er/poly-Si(n)/Al	Er Electroplating	Impact excitation	>10 V; >1 A cm ⁻²	Er: 1.54 μ m	–	<10 ⁻³ %	–	1997	[186]
Al/Si(p)/Si-rich SiO ₂ :Er/poly-Si(n)/Au	Er Electroplating	Impact excitation (reverse bias)	>18 V; >1.4 mA	Er: 1.54 μ m	–	EQE = 0.01%	Stable	1999	[187]
Si(p)/SiO _x + nc-Si:Er/Metal	Er Implantation	Impact excitation	–	Er: 1.54 μ m	–	IQE = 10%	100 h	2001	[188]
Si(p)/SiO _x + nc-Si:Tb /Metal	Tb Implantation	Impact excitation	–	Tb: 540 nm	–	IQE = 3%	100 h	2001	[188]
Si(p)/SiO _x + nc-Si:Er/Metal	Er Implantation	Impact excitation	–	Er: 1.54 μ m	1.4 kHz	1%	Stable	2002	[144]
Si(p ⁺)/SiO _x + nc-Si:Er/Metal	Er Implantation	–	0.06–20 mA cm ⁻²	Er: 1.54 μ m	1.15 kHz	–	–	2003	[189]
Si(p ⁺)/SiO _x i:Er/Metal	Er Implantation	Impact excitation	0.8–4,000 mA cm ⁻²	Er: 1.54 μ m	333 Hz	EQE = 10%	100 h	2003	[190]
Si(p ⁺)/SiO _x + nc-Si:Er/Metal	Er Implantation	Impact excitation	–	Er: 1.54 μ m	–	EQE = 1%	Stable	2003	[190]
Si(p ⁺)/SiO _x :Tb/Metal	Tb Implantation	Impact excitation	0.02–20 mA	Tb: 540 nm	–	EQE = 10%	–	2003	[190]
Si(p ⁺)/SiO _x :Yb/Metal	Yb Implantation	Impact excitation	0.1–10 mA	Yb: 980 nm	–	EQE = 0.1%	–	2003	[190]

EQE External quantum efficiency and IQE Internal quantum efficiency. Stated voltage and current are the minimum values for EL detection, or the device operation conditions

Tsybescov et al. [186] have obtained room temperature PL and EL from so-called Er-doped silicon-rich silicon oxide. PS made from p⁺ type Si was the starting material. PS was first doped by Er ions by electroplating and later converted to silicon-rich silicon oxide by partial thermal oxidation at 900°C. The LED structure is a n-i-p bipolar device with a 350-nm thick n-type poly-Si top contact, a 0.5 μm Er-doped silicon-rich silicon oxide, and a p-type c-Si substrate. The EL was detected under forward bias above 10 V and current density near 1 A cm⁻². The low efficiency (<10⁻⁴%) was attributed to the excitation of a small fraction of the Er ions only (volume concentration of Er ions was about 5 × 10¹⁸ cm⁻³). The excitation mechanism was believed to be impact of hot electrons.

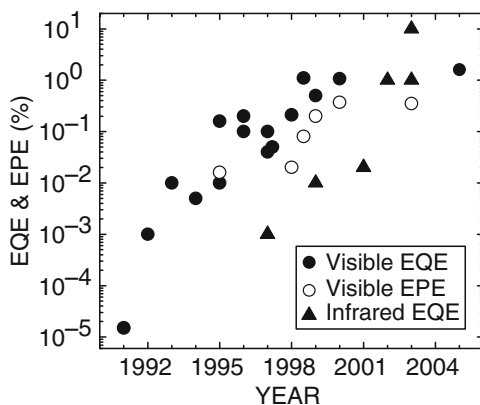
A similar LED based on Er-doped PS was later reported [187]. The volume concentration of Er ions was about 10¹⁹ cm⁻³. This time, stable EL was observed both under forward and reverse conditions. EQE of 0.01% was achieved for highest input powers. Temperature dependence of the EL led the author to conclude that, in reverse bias, the EL is a result of excitation by hot electrons, whereas excitation in forward bias occurs through an electron-hole-mediated recombination process as in PL.

Relatively high QEs, above 1%, have been reported using Er-doped Si nanoclusters embedded in MOS structures. Wang et al. [188] reported internal QEs of 10% and 3% for Er and Tb implanted MOS diodes, respectively. The EL excitation mechanism was hot electron impact. This process was progressively deteriorating the device oxide, resulting in about 100 h of stable operation.

In a typical device from a group that have been very active in this field [144, 189], a 70 nm thick SiO_x (x < 2) was deposited onto a low resistivity p-type Si substrate. Er was then implanted to a dose of 7 × 10¹⁴ cm⁻³. Samples were annealed at 900°C for 1 h in order to activate Er ions and to induce the separation of the Si and SiO₂ phases. The presence of the Si nanoclusters dispersed in the SiO₂ matrix makes Er electrical excitation efficient. The excitation cross section for Er under electrical pumping (10⁻¹⁴ cm²) was two orders of magnitude higher than the effective excitation cross section of Er through Si nanoclusters under optical pumping. Stable EL was obtained at room temperature with an estimated QE of 1%. EL rise and decay times were about 77 μs and 660 μs, respectively. A strong saturation of the EL intensity is possible under high injection condition because of saturation of the Er emitting centers. This could open the way to new optoelectronics applications.

Another group has also recently published very good results using MOS structures [190]. When Er is implanted into the gate oxide, an external QE of 10% has been achieved at RT. The EL mechanism, occurring by hot electrons impact, deteriorates the oxide. However, by using Si-rich oxide as gate dielectric, the devices show a high stability, the cost being the external QE reduced to 1%. The results of Sun et al. [191] support the fact that an increase of the Si nanocluster density causes direct tunneling of electrons between nanoclusters, reducing the population of energetic hot electrons for impact excitation, and therefore reducing the efficiency. The Er pumping occurs by energy transfer from the Si nanostructures to the rare-earth ions. Devices including Tb- and Yb-doped oxide were also reported [190]. These devices emitted EL at 540 nm (Tb) and 980 nm (Yb) with an

FIG. 14. Selected values of external quantum efficiencies (EQE) and external power efficiencies (EPE) of devices based on nc-Si. *Solid symbols* refer to quantum efficiencies whereas *hollow symbols* refer to power efficiencies. *Circles* refer to devices emitting visible light whereas *triangles* refer to devices emitting infrared light. Most data have been taken from the tables in this review.



external QE of 10% and 0.1%, respectively. A saturation of the EL intensity of Er- and Tb-based devices as a function of the current showed was observed for relatively low currents, from about 500 μ A.

8. CONCLUSION

In the past decade, the visible EL from Si has been extensively studied, in a view to achieving sufficient efficiency, brightness, and stability for applications. Figure 14 shows the evolution of the efficiency of devices based on nc-Si in recent past years. Basically, the efficiency has increased exponentially until the new millennium began. The 1% mark external QE has been reached [4, 5, 51] but it is difficult to achieve much better results for visible emitting devices, though rare-earth ions such as Tb could provide EQE up to 10% [190]. For devices emitting infrared light, particularly with Er ions, external QE of 10% has been achieved though the value remains at 1% for stable devices [144, 188–190]. Thus, infrared emitting devices seem the most promising for applications. These devices are very promising also because of possible lasing capabilities.

LEDs based on PS have been made efficient up to 1.1% in external QE and 0.37% in external power efficiency [4], as fast as 200 MHz [86], and stable during months of operation using surface chemical modification [6]. However, not any one LED could exhibit all these record characteristics at the same time. The major recent breakthroughs were the use of ECO to enhance the QE [4, 58], the chemical modification of the surface with organic molecule to enhance the stability [6, 82], and the HWA treatment to enhance both the QE and the stability [2, 3, 63]. The HWA is currently being investigated and is very promising for the quest of highly efficient and stable PS LEDs.

LEDs based on nc-Si in SiO_x matrix, and on other types of nanostructures exhibit external QE usually well below 1%. However, one device based on nc-Si in

SiN_x provided a record of 1.6% [5]. This shows that reasonably high efficiencies are possible in nc-Si devices.

Since high PL external QEs, well over 10%, have recently been reached [1–3] at RT for visible emission, the major challenge is now the carrier injection efficiency. A very promising injection scheme is the sequential injection in a floating-gate transistor structure [148].

The speed of Si-based LEDs is enough for display purposes but is far too low for interconnects. Thus, the most likely application of PS-based LED would be in display area, and other devices where speed is not an issue.

The ballistic electron emission from PS diodes is very promising for display applications. Prototypes have already been proven functional [105, 112]. Multicolor solid-state planar luminescent devices not requiring any vacuum intermediate region between the electron emitter and the luminescent phosphor has also been demonstrated [113–116].

REFERENCES

1. Y. Q. Wang, G. L. Kong, W. D. Chen, H. W. Diao, C. Y. Chen, S. B. Zhang and X. B. Liao, *Appl. Phys. Lett.* **81**, 4174 (2002)
2. B. Gelloz, A. Kojima and N. Koshida, *Appl. Phys. Lett.* **87**, 031107 (2005)
3. B. Gelloz and N. Koshida, *J. Appl. Phys.* **98**, 123509 (2005)
4. B. Gelloz and N. Koshida, *J. Appl. Phys.* **88**(7), 4319 (2000)
5. K. S. Cho, N. M. Park, T. Y. Kim, K. H. Kim, G. Y. Sung and J. H. Shin, *Appl. Phys. Lett.* **86**(7), 071909 (2005)
6. B. Gelloz, H. Sano, R. Boukherroub, D. D. M. Wayner, D. J. Lockwood and N. Koshida, *Appl. Phys. Lett.* **83**, 2342 (2003)
7. R. L. Smith and S. D. Collins, *J. Appl. Phys.* **71**, R1 (1992)
8. L. T. Canham, T. I. Cox, A. Loni and A. J. Simons, *Appl. Surf. Sci.* **102**, 436 (1996)
9. A. G. Cullis, L. T. Canham and P. D. J. Calcott, *J. Appl. Phys.* **82**, 909 (1997)
10. O. Bisi, S. Ossicini and L. Pavesi, *Surf. Sci. Rep.* **38**, 5 (2000)
11. M. V. Wolkin, J. Jorne, P. M. Fauchet, G. Allan and C. Delerue, *Phys. Rev. Lett.* **82**, 197 (1999)
12. H. Mizuno, H. Koyama and N. Koshida, *Thin Solid Films* **297**, 61 (1997)
13. H. Mizuno, H. Koyama and N. Koshida, *Appl. Phys. Lett.* **69**, 3779 (1996)
14. H. Mizuno and N. Koshida, *Mater. Res. Soc. Symp. Proc.* **536**, 179 (1999)
15. A. Halimaoui, C. Oules, G. Bomchil, A. Bsiesy, F. Gaspard, R. Herino, M. Ligeon and F. Muller, *Appl. Phys. Lett.* **59**, 304 (1991)
16. J. N. Chazalviel and F. Ozanam, *Mater. Res. Soc. Symp. Proc.* **283**, 359 (1992)
17. A. Bsiesy, J. C. Vial, F. Gaspard, R. Herino, M. Ligeon, F. Muller, R. Romestain, et al., *Surf. Sci.* **254**, 195 (1991)
18. M. A. Hory, R. Herino, M. Ligeon, F. Muller, F. Gaspard, I. Mihalcescu and J. C. Vial, *Thin Solid Films* **255**, 200 (1995)
19. J. L. Cantin, M. Schoisswohl, A. Grosman, S. Lebib, C. Ortega, H. J. Vonbardeleben, E. Vazsonyi, et al., *Thin Solid Films* **276**, 76 (1996)
20. S. Billat, *J. Electrochem. Soc.* **143**, 1055 (1996)
21. P. M. M. C. Bressers, J. W. J. Knapen, E. A. Meulenlamp and J. J. Kelly, *Appl. Phys. Lett.* **61**, 108 (1992)
22. L. T. Canham, W. Y. Leong, M. I. J. Beale, T. I. Cox and L. Taylor, *Appl. Phys. Lett.* **61**, 2563 (1992)

23. R. Memming, *J. Electrochem. Soc.* **116**, 785 (1969)
24. A. Bsiesy, F. Muller, M. Ligeon, F. Gaspard, R. Herino, R. Romestain and J. C. Vial, *Phys. Rev. Lett.* **71**, 637 (1993)
25. R. Romestain, J. C. Vial, I. Mihalcescu and A. Bsiesy, *Phys. Status Solidi B* **190**, 77 (1995)
26. A. Bsiesy and J. C. Vial, *J. Lumin.* **70**, 310 (1996)
27. B. Gelloz, A. Bsiesy and R. Herino, *J. Appl. Phys.* **94**, 2381 (2003)
28. E. S. Kooij, R. W. Despo and J. J. Kelly, *Appl. Phys. Lett.* **66**, 2552 (1995)
29. W. H. Green, E. J. Lee, J. M. Lauerhaas, T. W. Bitner and M. J. Sailor, *Appl. Phys. Lett.* **67**, 1468 (1995)
30. B. Gelloz and N. Koshida, *Jpn. J. Appl. Phys., Part 1* **43**, 1981 (2004)
31. A. Bsiesy, B. Gelloz, F. Gaspard and F. Muller, *J. Appl. Phys.* **79**, 2513 (1996)
32. B. Gelloz, A. Bsiesy, F. Gaspard and F. Muller, *Thin Solid Films* **276**, 175 (1996)
33. B. Gelloz, A. Bsiesy and R. Herino, *J. Lumin.* **82**, 205 (1999)
34. B. Gelloz and A. Bsiesy, *Appl. Surf. Sci.* **135**, 15 (1998)
35. B. Gelloz and A. Bsiesy, *Electrochem. Soc. Proc.* **97**, 92 (1997)
36. T. Oguro, H. Koyama, T. Ozaki and N. Koshida, *J. Appl. Phys.* **81**, 1407 (1997)
37. N. Koshida and H. Koyama, *Appl. Phys. Lett.* **60**, 347 (1992)
38. F. Namavar, H. P. Maruska and N. M. Kalkhoran, *Appl. Phys. Lett.* **60**, 2514 (1992)
39. H. P. Maruska, F. Namavar and N. M. Kalkhoran, *Appl. Phys. Lett.* **61**, 1338 (1992)
40. F. Kozlowski, M. Sauter, P. Steiner, A. Richter, H. Sandmaier and W. Lang, *Thin Solid Films* **222**, 196 (1992)
41. A. Grosman and C. Ortega, in *Properties of Porous Silicon*, edited by L. T. Canham (INSPEC, The Institution of Electrical Engineers, London, 1997), vol. 18, pp. 328–335
42. J. Linnros and N. Lalic, *Appl. Phys. Lett.* **66**, 3048 (1995)
43. N. Lalic and J. Linnros, *J. Appl. Phys.* **80**, 5971 (1996)
44. N. Lalic and J. Linnros, *Thin Solid Films* **276**, 155 (1996)
45. P. Steiner, F. Kozlowski and W. Lang, *Appl. Phys. Lett.* **62**, 2700 (1993)
46. A. Loni, A. J. Simons, T. I. Cox, P. D. J. Calcott and L. T. Canham, *Electron. Lett.* **31**, 1288 (1995)
47. W. Lang, F. Kozlowski, P. Steiner, B. Knoll, A. Wiedenhofer, D. Kollewe and T. Bachmann, *Thin Solid Films* **297**, 268 (1997)
48. K. Nishimura, Y. Nagao and N. Ikeda, *Jpn. J. Appl. Phys., Part 2* **37**, L303 (1998)
49. C. Peng and P. M. Fauchet, *Appl. Phys. Lett.* **67**, 2515 (1995)
50. Z. L. Chen, G. Bosman and R. Ochoa, *Appl. Phys. Lett.* **62**, 708 (1993)
51. B. Gelloz, T. Nakagawa and N. Koshida, *Mater. Res. Soc. Symp. Proc.* **536**, 15 (1998)
52. A. Simons, T. I. Cox, A. Loni, L. T. Canham, M. J. Uren, C. Reeves, A. G. Cullis, et al., *Electrochem. Soc. Proc.* **95**, 73 (1997)
53. T. I. Cox, A. J. Simons, A. Loni, P. D. J. Calcott, L. T. Canham, M. J. Uren and K. J. Nash, *J. Appl. Phys.* **86**, 2764 (1999)
54. F. Kozlowski, W. Wagenseil, P. Steiner and W. Lang, *Mater. Res. Soc. Symp. Proc.* **358**, 677 (1995)
55. P. M. Fauchet, L. Tsybeskov, S. P. Duttagupta and K. D. Hirschman, *Thin Solid Films* **297**, 254 (1997)
56. L. Tsybeskov, S. P. Duttagupta, K. D. Hirschman and P. M. Fauchet, *Appl. Phys. Lett.* **68**, 2058 (1996)
57. L. Tsybeskov, S. P. Duttagupta and P. M. Fauchet, *Solid State Commun.* **95**, 429 (1995)
58. B. Gelloz, T. Nakagawa and N. Koshida, *Appl. Phys. Lett.* **73**, 2021 (1998)
59. L. Pavesi, R. Chierchia, P. Bellutti, A. Lui, F. Fuso, M. Labardi, L. Pardi, et al., *J. Appl. Phys.* **86**, 6474 (1999)
60. B. Gelloz and N. Koshida, *Electrochem. Soc. Proc.* **99**, 27 (1999)
61. K. D. Hirschman, L. Tsybeskov, S. P. Duttagupta and P. M. Fauchet, *Nature* **384**, 338 (1996)
62. H. Mimura, T. Matsumoto and Y. Kanemitsu, *J. Non-Cryst. Solids* **200**, 961 (1996)
63. B. Gelloz and N. Koshida, *Jpn. J. Appl. Phys., Part 1* **45**, 3462 (2006)

64. P. Steiner, F. Kozlowski, M. Wielunski and W. Lang, *Jpn. J. Appl. Phys.*, Part 1 **33**, 6075 (1994)
65. P. Steiner, A. Wiedenhofer, F. Kozlowski and W. Lang, *Thin Solid Films* **276**, 159 (1996)
66. N. Koshida, H. Koyama, Y. Yamamoto and G. J. Collins, *Appl. Phys. Lett.* **63**, 2655 (1993)
67. N. Koshida, H. Mizuno, H. Koyama and G. J. Collins, *Jpn. J. Appl. Phys.*, Part 2 **34**, 92 (1994)
68. A. Bsiesy, Y. F. Nicolau, A. Ermoloeff, F. Muller and F. Gaspard, *Thin Solid Films* **255**, 43 (1995)
69. D. P. Halliday, E. R. Holland, J. M. Eggleston, P. N. Adams, S. E. Cox and A. P. Monkman, *Thin Solid Films* **276**, 299 (1996)
70. K. H. Li, D. C. Diaz, Y. S. He, J. C. Campbell and C. C. Tsai, *Appl. Phys. Lett.* **64**, 2394 (1994)
71. A. J. Simons, T. I. Cox, A. Loni, L. T. Canham and R. Blacker, *Thin Solid Films* **297**, 281 (1997)
72. S. Lazarouk, P. Jaguiro, S. Katsouba, G. Masini, S. Lamonica, G. Maiello and A. Ferrari, *Appl. Phys. Lett.* **68**, 2108 (1996)
73. S. Lazarouk, P. Jaguiro, S. Katsouba, S. Lamonica, G. Maiello, G. Masini and A. Ferrari, *Thin Solid Films* **276**, 168 (1996)
74. F. Kozlowski, C. Sailer, P. Steiner, B. Knoll and W. Lang, *Thin Solid Films* **276**, 164 (1996)
75. Y. A. Chen, B. F. Chen, W. C. Tsay, L. H. Lai, M. N. Chang, J. I. Chyi, J. W. Hong and C. Y. Chang, *Solid-State Electron.* **41**, 757 (1997)
76. Y. A. Chen, N. Y. Liang, L. H. Lai, W. C. Tsay, M. N. Chang and J. W. Hong, *Jpn. J. Appl. Phys.*, Part 1 **36**, 1574 (1997)
77. Y. A. Chen, N. Y. Liang, L. H. Lai, W. C. Tsay, M. N. Chang and J. W. Hong, *Electron. Lett.* **33**, 1489 (1997)
78. T. Futagi, T. Matsumoto, M. Katsuno, Y. Ohta, H. Mimura and K. Kitamura, *Jpn. J. Appl. Phys.*, Part 2 **31**, L616 (1992)
79. N. Koshida, J. Kadokura, M. Takahashi and K. Imai, *Mater. Res. Soc. Symp. Proc.* **638**, F18.3.1 (2001)
80. T. Matsumoto, Y. Masumoto, T. Nakagawa, M. Hashimoto, K. Ueno and N. Koshida, *Jpn. J. Appl. Phys.*, Part 2 **36**, L1089 (1997)
81. J. M. Buriak, *Chem. Rev.* **102**, 1271 (2002)
82. B. Gelloz, H. Sano, R. Boukhrroub, D. D. M. Wayner, D. J. Lockwood and N. Koshida, *Phys. Status Solidi C* **2**, 3273 (2005)
83. L. Pavesi, R. Guardini and C. Mazzoleni, *Solid State Commun.* **97**, 1051 (1996)
84. S. Chan and P. M. Fauchet, *Appl. Phys. Lett.* **75**(2), 274 (1999)
85. M. Araki, H. Koyama and N. Koshida, *Appl. Phys. Lett.* **69**, 2956 (1996)
86. M. Balucani, S. La Monica and A. Ferrari, *Appl. Phys. Lett.* **72**, 639 (1998)
87. M. Takahashi and N. Koshida, *J. Appl. Phys.* **86**, 5274 (1999)
88. M. G. Berger, R. Arensfischer, M. Thonissen, M. Kruger, S. Billat, H. Luth, S. Hilbrich, et al., *Thin Solid Films* **297**, 237 (1997)
89. S. Frohnhoff and M. G. Berger, *Adv. Mater.* **6**, 963 (1994)
90. K. Ueno and N. Koshida, *Appl. Phys. Lett.* **74**, 93 (1999)
91. K. Ueno and N. Koshida, *Jpn. J. Appl. Phys.*, Part 1 **37**, 1096 (1998)
92. M. Takahashi, Y. Toriumi, T. Matsumoto, Y. Masumoto and N. Koshida, *Appl. Phys. Lett.* **76**, 1990 (2000)
93. N. Koshida, E. Takizawa, H. Mizuno, S. Arai, H. Koyama and T. Sameshima, *Mater. Res. Soc. Symp. Proc.* **486**, 151 (1998)
94. A. El-Bahar and Y. Nemirovsky, *Appl. Phys. Lett.* **77**, 208 (2000)
95. G. Barillaro, A. Diligenti, F. Pieri, F. Fuso and M. Allegrini, *Appl. Phys. Lett.* **78**, 4154 (2001)
96. L. Li, B. Gelloz and N. Koshida, Meeting Abstracts, International Semiconductor Technology Conference ISTC (Tokyo, 2002), Abstract No. 37.
97. N. Koshida, T. Ozaki, X. Sheng and H. Koyama, *Jpn. J. Appl. Phys.*, Part 2 **34**, L705 (1995)
98. X. Sheng, T. Ozaki, H. Koyama, N. Koshida, T. Yoshikawa, M. Yamaguchi and K. Ogasawara, *Thin Solid Films* **297**, 314 (1997)

99. X. Sheng, H. Koyama, N. Koshida, S. Iwasaki, N. Negishi, T. Chuman, T. Yoshikawa and K. Ogasawara, *J. Vac. Sci. Technol. B* **15**, 1661 (1997)
100. X. Sheng, H. Koyama and N. Koshida, *J. Vac. Sci. Technol. B* **16**, 793 (1998)
101. N. Koshida, X. Sheng and T. Komoda, *Appl. Surf. Sci.* **146**, 371 (1999)
102. T. Komoda, X. Sheng and N. Koshida, *J. Vac. Sci. Technol. B* **17**, 1076 (1999)
103. T. Komoda, Y. Honda, T. Hatai, Y. Watanabe, T. Ichihara, K. Aizawa, Y. Kondo, et al., *IDW'99* **939** (1999)
104. T. Komoda, T. Ichihara, Y. Honda, K. Aizawa and N. Koshida, *Mater. Res. Soc. Symp. Proc.* **638**, F4.1.1 (2001)
105. T. Komoda, Y. Honda, T. Ichihara, T. Hatai, Y. Takegawa, Y. Watanabe, K. Aizawa, et al., *SID '02 Digest* **33**, 1128 (2002)
106. C. A. Spindt, C. E. Holland, A. Rosengreen and I. Brodie, *J. Vac. Sci. Technol. B* **11**, 468 (1993)
107. C. A. Spindt, *J. Appl. Phys.* **39**, 3504 (1968)
108. K. Yokoo, H. Tanaka, S. Sato, J. Murota and S. Ono, *J. Vac. Sci. Technol. B* **11**, 429 (1993)
109. M. Suzuki and T. Kusunoki, *IDW'96* **529** (1996)
110. A. Kojima and N. Koshida, *Appl. Phys. Lett.* **86**, (2005)
111. A. Kojima, X. Sheng and N. Koshida, *Mater. Res. Soc. Symp. Proc.* **638**, F3.31 (2001)
112. T. Komoda, T. Ichihara, Y. Honda, T. Hatai, T. Baba, Y. Takegawa, Y. Watabe, et al., *J. Soc. Inf. Display* **12**, 29 (2004)
113. Y. Nakajima, A. Kojima, H. Toyama and N. Koshida, *Jpn. J. Appl. Phys., Part 1* **41**, 2707 (2002)
114. Y. Nakajima, A. Kojima and N. Koshida, *Appl. Phys. Lett.* **81**(13), 2472 (2002)
115. Y. Nakajima, A. Kojima and N. Koshida, *Mater. Res. Soc. Symp. Proc.* **638**, F4.2.1 (2001)
116. Y. Nakajima, T. Uchida, H. Toyama, A. Kojima, B. Gelloz and N. Koshida, *Jpn. J. Appl. Phys., Part 1* **43**, 2076 (2004)
117. B. Gelloz, T. Kanda, T. Uchida, M. Niibe, A. Kojima and N. Koshida, *Jpn. J. Appl. Phys., Part 1* **44**, 2676 (2005)
118. L. Pavesi, L. Dal Negro, C. Mazzoleni, G. Franzo and F. Priolo, *Nature* **408**, 440 (2000)
119. F. Iacona, G. Franzo and C. Spinella, *J. Appl. Phys.* **87**, 1295 (2000)
120. T. Inokuma, Y. Wakayama, T. Muramoto, R. Aoki, Y. Kurata and S. Hasegawa, *J. Appl. Phys.* **83**, 2228 (1998)
121. Q. Zhang, S. C. Bayliss and D. A. Hutt, *Appl. Phys. Lett.* **66**, 1977 (1995)
122. S. Hayashi, T. Nagareda, Y. Kanzawa and K. Yamamoto, *Jpn. J. Appl. Phys., Part 1* **32**, 3840 (1993)
123. T. Shimizuiwayama, S. Nakao and K. Saitoh, *Appl. Phys. Lett.* **65**, 1814 (1994)
124. J. G. Zhu, C. W. White, J. D. Budai, S. P. Withrow and Y. Chen, *J. Appl. Phys.* **78**, 4386 (1995)
125. K. S. Min, K. V. Shcheglov, C. M. Yang, H. A. Atwater, M. L. Brongersma and A. Polman, *Appl. Phys. Lett.* **69**, 2033 (1996)
126. J. Linnros, N. Lalic, A. Galeckas and V. Grivickas, *J. Appl. Phys.* **86**, 6128 (1999)
127. I. Sychugov, R. Juhasz, J. Valenta and J. Linnros, *Phys. Rev. Lett.* **94**, (2005)
128. I. Sychugov, R. Juhasz, J. Linnros and J. Valenta, *Phys. Rev. B* **71**, (2005)
129. I. Sychugov, R. Juhasz, A. Galeckas, J. Valenta and J. Linnros, *Opt. Mater.* **27**, 973 (2005)
130. J. Valenta, R. Juhasz and J. Linnros, *Appl. Phys. Lett.* **80**, 1070 (2002)
131. J. Valenta, N. Lalic and J. Linnros, *Appl. Phys. Lett.* **84**, 1459 (2004)
132. H. Z. Song, X. M. Bao, N. S. Li and J. Y. Zhang, *J. Appl. Phys.* **82**, 4028 (1997)
133. K. Luterova, I. Pelant, J. Valenta, J. L. Rehspringer, D. Muller, J. J. Grob, J. Dian and B. Honerlage, *Appl. Phys. Lett.* **77**, 2952 (2000)
134. N. Lalic and J. Linnros, *J. Lumin.* **80**, 263 (1998)
135. V. Ovchinnikov, S. Novikov, T. Toivola and J. Sinkkonen, *Microelectron. J.* **36**, 502 (2005)
136. J. De La Torre, A. Souifi, A. Poncet, C. Busseret, M. Lemiti, G. Bremond, G. Guillot, et al., *Phys. E* **16**, 326 (2003)
137. J. De La Torre, A. Souifi, M. Lemiti, A. Poncet, C. Busseret, G. Guillot, G. Bremond, et al., *Phys. E* **17**(1–4), 604 (2003)
138. G. R. Lin, C. J. Lin, C. K. Lin, L. J. Chou and Y. L. Chueh, *J. Appl. Phys.* **97**, (2005)

139. G. G. Qin, A. P. Li, B. R. Zhang and B. C. Li, *J. Appl. Phys.* **78**, 2006 (1995)
140. A. Irrera, D. Pacifici, M. Miritello, G. Franzo, F. Priolo, F. Iacona, D. Sanfilippo, et al., *Appl. Phys. Lett.* **81**, 1866 (2002)
141. A. Irrera, D. Pacifici, M. Miritello, G. Franzo, F. Priolo, F. Iacona, D. Sanfilippo, et al., *Phys. E* **16**, 395 (2003)
142. G. Franzo, A. Irrera, E. C. Moreira, M. Miritello, F. Iacona, D. Sanfilippo, G. Di Stefano, et al., *Appl. Phys. A* **74**, 1 (2002)
143. A. Irrera, F. Iacona, G. Franzo, S. Boninelli, D. Pacifici, M. Miritello, C. Spinella, et al., *Opt. Mater.* **27**(5), 1031 (2005)
144. F. Iacona, D. Pacifici, A. Irrera, M. Miritello, G. Franzo, F. Priolo, D. Sanfilippo, et al., *Appl. Phys. Lett.* **81**, 3242 (2002)
145. G. G. Qin, Y. Q. Wang, Y. P. Qiao, B. R. Zhang, Z. C. Ma and W. H. Zong, *Appl. Phys. Lett.* **74**, 2182 (1999)
146. C. L. Heng, Y. K. Sun, S. T. Wang, Y. Chen, Y. P. Qiao, B. R. Zhang, Z. C. Ma, et al., *Appl. Phys. Lett.* **77**, 1416 (2000)
147. P. Photopoulos and A. G. Nassiopoulou, *Appl. Phys. Lett.* **77**, 1816 (2000)
148. R. J. Walters, G. I. Bourianoff and H. A. Atwater, *Nature Mater.* **4**(2), 143 (2005)
149. N. M. Park, T. S. Kim and S. J. Park, *Appl. Phys. Lett.* **78**, 2575 (2001)
150. L. Y. Chen, W. H. Chen and F. C. N. Hong, *Appl. Phys. Lett.* **86**, (2005)
151. A. G. Nassiopoulos, S. Grigoropoulos and D. Papadimitriou, *Appl. Phys. Lett.* **69**, 2267 (1996)
152. A. G. Nassiopoulos, S. Grigoropoulos and D. Papadimitriou, *Thin Solid Films* **297**, 176 (1997)
153. S. Tong, X. N. Liu, L. C. Wang, F. Yan and X. M. Bao, *Appl. Phys. Lett.* **69**, 596 (1996)
154. S. Fujita and N. Sugiyama, *Appl. Phys. Lett.* **74**, 308 (1999)
155. T. Yoshida, Y. Yamada and T. Orii, *J. Appl. Phys.* **83**, 5427 (1998)
156. T. Makino, Y. Yamada, N. Suzuki, T. Yoshida and S. Onari, *J. Appl. Phys.* **90**, 5075 (2001)
157. T. Makino, Y. Yamada, N. Suzuki, T. Yoshida and S. Onari, *Appl. Surf. Sci.* **197**, 594 (2002)
158. T. Toyama, Y. Kotani, H. Okamoto and H. Kida, *Appl. Phys. Lett.* **72**, 1489 (1998)
159. Y. Osaka, K. Kohno, H. Mizuno and N. Koshida, *Jpn. J. Appl. Phys., Part 1* **41**, 7481 (2002)
160. W. L. Ng, M. A. Lourenco, R. M. Gwilliam, S. Ledain, G. Shao and K. P. Homewood, *Nature* **410**, 192 (2001)
161. M. Kittler, T. Argyurov, A. Fischer and W. Seifert, *Opt. Mater.* **27**, 967 (2005)
162. J. M. Sun, T. Dekorsy, W. Skorupa, A. Mucklich, B. Schmidt and M. Helm, *Opt. Mater.* **27**, 1041 (2005)
163. M. J. Chen, J. L. Yen, J. Y. Li, J. F. Chang, S. C. Tsai and C. S. Tsai, *Appl. Phys. Lett.* **84**, 2163 (2004)
164. R. Tsu, A. Filios, C. Lofgren, K. Dovidenko and C. G. Wang, *Electrochem. Solid State Lett.* **1**, 80 (1998)
165. L. Heikkila, T. Kuusela and H. P. Hedman, *Superlattices and Microstructures* **26**, 157 (1999)
166. L. Heikkila, T. Kuusela and H. P. Hedman, *J. Appl. Phys.* **89**, 2179 (2001)
167. P. Photopoulos, A. G. Nassiopoulou, D. N. Kouvatsos and A. Travlos, *Mater. Sci. Eng. B* **69**, 345 (2000)
168. Z. Gaburro, L. Pavesi, G. Pucker and P. Bellutti, *Mater. Res. Soc. Proc.* **638**, F18.5.1 (2001)
169. Z. Gaburro, G. Pucker, P. Bellutti and L. Pavesi, *Solid State Commun.* **114**, 33 (2000)
170. C. L. Heng, Y. Chen, Z. C. Ma, W. H. Zong and G. G. Qin, *J. Appl. Phys.* **89**, 5682 (2001)
171. S. Y. Ma, *Thin Solid Films* **402**, 222 (2002)
172. B. Averboukh, R. Huber, K. W. Cheah, Y. R. Shen, G. G. Qin, Z. C. Ma and W. H. Zong, *J. Appl. Phys.* **92**, 3564 (2002)
173. O. Jambois, H. Rinnert, X. Devaux and M. Vergnat, *J. Appl. Phys.* **98**(4), 046105 (2005)
174. W. Wu, X. F. Huang, K. J. Chen, J. B. Xu, X. Gao, J. Xu and W. Li, *J. Vac. Sci. Technol. A* **17**, 159 (1999)
175. F. A. Davitaya, L. Vervoort, F. Bassani, S. Ossicini, A. Fasolino and F. Bernardini, *Europhys. Lett.* **31**, 25 (1995)

176. L. Vervoort, F. Bassani, I. Mihalcescu, J. C. Vial and F. A. Davitaya, *Phys. Status Solidi B* **190**, 123 (1995)
177. A. B. Filonov, A. N. Kholod, V. A. Novikov, V. E. Borisenko, L. Vervoort, F. Bassani, A. Saul and F. A. Davitaya, *Appl. Phys. Lett.* **70**, 744 (1997)
178. V. Ioannou-Sougleridis, V. Tsakiri, A. G. Nassiopoulou, P. Photopoulos, F. Bassani and F. A. D'avitaya, *Phys. Status Solidi A* **165**, 97 (1998)
179. A. N. Kholod, A. L. Danilyuk, V. E. Borisenko, F. Bassani, S. Menard and F. A. D'avitaya, *J. Appl. Phys.* **85**, 7219 (1999)
180. T. Maruyama, N. Nakamura and M. Watanabe, *Jpn. J. Appl. Phys., Part 1* **39**, 1996 (2000)
181. T. Maruyama, N. Nakamura and M. Watanabe, *Jpn. J. Appl. Phys., Part 2* **38**, L904 (1999)
182. V. Ioannou-Sougleridis, A. G. Nassiopoulou, T. Ouisse, F. Bassani and F. A. D'avitaya, *Appl. Phys. Lett.* **79**, 2076 (2001)
183. V. Ioannou-Sougleridis, T. Ouisse, A. G. Nassiopoulou, F. Bassani and F. A. D'avitaya, *J. Appl. Phys.* **89**, 610 (2001)
184. G. Franzo, D. Pacifici, V. Vinciguerra, F. Priolo and F. Iacona, *Appl. Phys. Lett.* **76**, 2167 (2000)
185. M. Zacharias, J. Heitmann, M. Schmidt and P. Streitenberger, *Phys. E* **11**, 245 (2001)
186. L. Tsybeskov, S. P. Duttagupta, K. D. Hirschman, P. M. Fauchet, K. L. Moore and D. G. Hall, *Appl. Phys. Lett.* **70**, 1790 (1997)
187. H. A. Lopez and P. M. Fauchet, *Appl. Phys. Lett.* **75**, 3989 (1999)
188. S. Wang, S. Coffa, R. Carius and C. Buchal, *Mater. Sci. Eng. B* **81**, 102 (2001)
189. D. Pacifici, A. Irrera, G. Franzo, M. Miritello, F. Iacona and F. Priolo, *Phys. E* **16**, 331 (2003)
190. M. E. Castagna, S. Coffa, M. Monaco, L. Caristia, A. Messina, R. Mangano and C. Bongiorno, *Phys. E* **16**, 547 (2003)
191. J. M. Sun, W. Skorupa, T. Dekorsy, M. Helm and A. N. Nazarov, *Opt. Mater.* **27**, 1050 (2005)

Device Applications of Silicon Nanocrystals and
Nanostructures

Koshida, N. (Ed.)

2009, XII, 344 p., Hardcover

ISBN: 978-0-387-78688-9